(*Oct3/4*), sex-determining region Y-box 2 (*Sox2*), Krüppel-like factor 4 (*Klf4*), and the v-Myc avian myelocytomatosis viral oncogene homolog (*c-Myc*) (Takahashi and Yamanaka, 2006; Meissner et al., 2007; Okita et al., 2007; Park et al., 2007; Takahashi et al., 2007; Yu et al., 2007; Aoi et al., 2008; Hanna et al., 2008; Nakagawa et al., 2008). The cloned cells display properties of self-renewal and pluripotency similar to ES cells, and yield germ-line adult chimeras. However, because iPS cells are "unnatural" cells that are reprogrammed from once-differentiated cells, their differentiation processes must first be analyzed and compared before any true relationship between iPS and ES cells can be made.

The concept of patient-specific stem cells is of great clinical interest, and has engendered considerable research within the scientific community. The applications of these cells are expected to contribute to patient-oriented disease investigations, drug screenings, toxicology, and transplantation therapies (Jaenisch and Young, 2008). For example, a recent study demonstrated that autologous iPS cells can be used to treat mice with sickle cell anemia (Hanna et al., 2007). Despite such encouraging results, little is known about the in vitro hematopoietic differentiation of iPS cells. In particular, it is currently unclear whether iPS and undifferentiated embryonic cells follow the same process toward hematopoietic commitment.

In this study, we compared the hematopoietic differentiation of iPS and ES cells in vitro during their coculture with OP9 stromal cells (Nakano et al., 1994, 1996; Umeda et al., 2004, 2006; Vodyanik et al., 2005; Shinoda et al., 2007; Vodyanik and Slukvin, 2007). Sequential fluorescence-activated cell sorting (FACS), immunostaining, and reverse transcription (RT)-polymerase chain reaction (PCR) analyses demonstrated that iPS cell-derived hematopoietic and endothelial cells emerge from a common mesodermal progenitor that is positive for Flk-1, as is the case in ES cells and in normal embryogenesis.

Materials and Methods

Generation of iPS cells

Murine iPS cells were established from murine fibroblasts as described previously (Takahashi and Yamanaka, 2006; Okita et al., 2007; Nakagawa et al., 2008). In brief, to generate Nanog-iPS cells (clones 20D17, 38C2, and 38D2), murine embryonic fibroblasts carrying the Nanog-GFP-IRES-Puro^r reporter were incubated in retrovirus-containing supernatants for Oct3/4, Sox2, Klf4, and c-Myc for 24 h. After 2–3 weeks, clones were selected for expansion in medium containing 1.5 μg/ml of puromycin. To generate three-factor (without c-Myc) iPS cells (clone 256H18), murine tail tip fibroblasts (TTFs) were first isolated from adult *Discosoma* sp. red fluorescent protein (DsRed)-transgenic mice. Retrovirus containing supernatants for Oct3/4, Sox2, Klf4, and GFP were then added to the TTF cultures for 24 h. Four days after transduction, TTFs were replated on SIM mouse embryo-derived thioguanine and ouabain-resistant (STO)-derived feeder cells producing leukemia inhibitory factor (LIF; designated as SNL cells). Thirty days after transduction, the colonies were selected for expansion.

Maintenance of cells

The iPS cells and the murine ES cell line D3 were maintained on confluent SNL cells at a concentration of 1×10^4 cells/cm^2 in Dulbecco's modified Eagle's medium (DMEM; Sigma–Aldrich, St. Louis, MO), containing 15% fetal calf serum (FCS; Sigma–Aldrich) and 0.1 μM 2-mercaptoethanol (2ME) (Takahashi and Yamanaka, 2006; Okita et al., 2007; Nakagawa et al., 2008). OP9 stromal cells, which were a kind gift from Dr. Kodama (Osaka University, Osaka), were maintained as reported previously (Umeda et al., 2004).

Antibodies

The primary antibodies used for flow cytometric (FCM) analysis included an unconjugated anti-stage-specific mouse embryonic antigen (SSEA1) mouse monoclonal immunoglobulin M (IgM) antibody (sc-21702; Santa Cruz Biotechnology, Santa Cruz, CA), and the following anti-mouse antibodies from Becton–Dickinson (Franklin Lakes, NJ): unconjugated rat monoclonal anti-E-cadherin, rat monoclonal allophycocyanin (APC)-conjugated anti-c-kit, unconjugated rat monoclonal anti-spinocerebellar ataxia type 1 (Sca1), unconjugated rat monoclonal anti-CD31, biotin-conjugated anti-Flk-1, biotin-conjugated anti-CD34, and biotin-conjugated anti-CD45. Two secondary antibodies against the unlabeled primary antibodies were also from Becton–Dickinson: an APC-conjugated anti-mouse IgM antibody and an APC-conjugated anti-rat IgG antibody.

The primary antibodies used to immunostain the floating erythrocytes included rabbit anti-mouse embryonic hemoglobin (a gift from Dr. Atsumi, Miwa et al., 1991) and rat anti-mouse hemoglobin β (sc31116; Santa Cruz Biotechnology). Cy3-conjugated goat anti-rabbit or anti-rat antibodies (Jackson ImmunoResearch Laboratories, Inc., West Grove, PA) were used as secondary antibodies.

The primary antibodies for immunostaining endothelial cells included anti-mouse antibodies from BD (Becton–Dickinson), an unconjugated anti-VE-cadherin rat monoclonal antibody, an unconjugated anti-CD31 rat monoclonal antibody, and an anti-eNOS rat monoclonal antibody. Horseradish peroxidase (HRP)-conjugated goat anti-rat antibodies (Jackson ImmunoResearch Laboratories, Inc.) were used as secondary antibodies.

Cytostaining

Floating cells were centrifuged onto glass slides using a Shandon Cytospin® 4 Cytocentrifuge (Thermo, Pittsburgh, PA), and analyzed by microscopy after staining with May–Giemsa, myeloperoxidase (MPO), or acetylcholine esterase (Maherali et al., 2007). Staining was performed as described previously (Jackson, 1973; Yang et al., 1999; Xu et al., 2001). For immunofluorescence staining, cells fixed with 4% paraformaldehyde (PFA) were first permeabilized with phosphate-buffered saline (PBS) containing 5% skimmed milk (Becton–Dickinson) and 0.1% Triton X-100, and then incubated with primary antibodies against embryonic or β-major globins, followed by incubation with Cy3-conjugated secondary antibodies. Nuclei were counterstained with 4,6-diamidino-2-phenylindole (Sigma–Aldrich). Fluorescence was detected and images obtained with an AxioCam photomicroscope (Carl Zeiss Vision GmbH, Hallbergmoos, Germany).

FACS

The adherent cells were treated with 0.25% trypsin/ethylenediaminetetraacetic acid (EDTA) and harvested. They were incubated in a new tissue-culture dish (Becton–Dickinson) for 30 min to eliminate adherent OP9 cells (Suwabe et al., 1998). Floating cells were then collected and stained with primary antibodies, followed by incubation with APC-conjugated anti-mouse IgM or anti-rat IgG antibodies. Dead cells were excluded by propidium iodide (Kyba et al., 2002, 2003) staining. Samples were analyzed using a FACSCalibur and Cell Quest software (Becton–Dickinson). Cell sorting with the Flk-1 antibody was performed using a FACSVantage flow cytometer (Becton–Dickinson).

Differentiation of iPS and ES cells

For initial differentiation, iPS or ES cells were treated with 0.25% trypsin/EDTA (Gibco, Grand Island, NY) and transferred onto semi-confluent OP9 cell layers at a concentration of 6×10^3 cells/cm^2 in α-minimum essential medium (α-MEM;

Gibco) supplemented with 10% FCS and 5×10^{-2} μM 2ME and without LIF. After 5 days, the induced cells were treated with 0.25% trypsin/EDTA, and 1.2×10^4 total cells/cm^2 or 1.2×10^3 sorted Flk-1$^+$ cells/cm^2 were transferred onto fresh semi-confluent OP9 cell layers, and cultured thereafter for hematopoietic differentiation in α-MEM supplemented with 10% FCS, 5×10^{-2} μM 2ME, and the following four recombinant growth factors: 100 ng/ml mouse stem-cell factor (mSCF), 4 ng/ml human thrombopoietin (hTPO), 20 ng/ml mouse interleukin 3 (mIL3), and 2 U/ml human erythropoietin (hEPO). These cytokines were kindly provided by Kirin Brewery (Tokyo, Japan).

RNA extraction and RT-PCR analysis

RNA samples were prepared using silica gel membrane-based spin-columns (RNeasy Mini-Kit™; Qiagen, Valencia, CA) and subjected to RT with a Sensiscript-RT Kit™ (Qiagen). All procedures were performed following the manufacturer's instructions. For RT-PCR, yields were adjusted by dilution to produce equal amounts of the glyceraldehyde-3-phosphate dehydrogenase (GAPDH) amplicon. Complementary DNA (cDNA) templates were initially denatured at 94°C for 5 min, followed by 29–35 amplification reactions consisting of 94°C for 15 sec (denaturing), 55–64°C for 15 sec (annealing), and 72°C for 30 sec (extension), with a final extension at 94°C for 7 min. The oligonucleotide primers were as follows: *GAPDH*, 5′-TCC AGA GGG GCC ATC CAC AGT C-3′ and 5′-GTC GGT GTG AAC GGA TTT GGC C-3′ (Baba et al., 2007a); *Rex1*, 5′-AAA GTG AGA TTA GCC CCG AG-3′ and 5′-TCC CAT CCC CTT CAA TAG CA-3′ (Baba et al., 2007a); *Brachyury*, 5′-CAT GTA CTC TTT CTT GCT GG-3′ and 5′-GGT CTC GGG AAA GCA GTG GC-3′ (Ku et al., 2004); *Flk-1*, 5′-CAC CTG GCA CTC TCC ACC TTC-3′ and 5′-GAT TTC ATC CCA CTA CCG AAA G-3′ (Baba et al., 2007a); *Scl*, 5′-ATG GAG ATT TCT GAT GGT CCT CAC-3′ and 5′-AAG TGT GCT TGG GTG TTG GCT C-3′ (Baba et al., 2007a); *Myb*, 5′-CAC CAT TCT GGA CAA TGT TAA GAA C-3′ and 5′-GTA AGG TAG GTG CAT CTA AGC-3′; *Tie1*, 5′-ATA CCC TAG ACT GGC AAG AG-3′ and 5′-TTT TGA CAC TGG CAC TGG A-3′; *Gata1*, 5′-GCT GAA TCC TCT GCA TCA AC-3′ and 5′-TAG GCC TCA GCT TCT CTG TA-3′ (Shimizu et al., 2001); *Gata2*, 5′-GCA ACA CAC CAC CCG ATA CC-3′ and 5′-CAA TTT GCA CAA CAG GTG CCC-3′ (Shimizu et al., 2004); *ε-globin*, 5′-GGA GAG TCC ATT AAG AAC CTA GAC AA-3′ and 5′-CTG TGA ATT CAT TGC CGA AGT GAC-3′ (Hansen et al., 1982); *ζ-globin*, 5′-GCT CAG GCC GAG CCC ATT GG-3′ and 5′-TAG CGG TAC TTC TCA GTC AG-3′ (Leder et al., 1985); *α-globin*, 5′-CTC TCT GGG GAA GAC AAA AGC AAC-3′ and 5′-GGT GGC TAG CCA AGG TCA CCA GCA-3′ (Nishioka and Leder, 1979); *β-globin*, 5′-CTG ACA GAT GCT CTC TTG GG-3′ and 5′-CAC AAC CCC AGA AAC AGA CA-3′ (Konkel et al., 1978); *Oct3/4* (Tg), 5′-AAA AAG CAG GCT CCA CCT TCC CCA TGG CTG GAC ACC-3′ and 5′-AGA AAG CTG GGT TGA TCA ACA GCA TCA CTG AGC TTC-3′ (Takahashi and Yamanaka, 2006); *Sox2* (Tg), 5′-AAA AAG CAG GCT TGT ATA ACA TGA TGG AGA CGG-3′ and 5′-AGA AAG CTG GGT TTC ACA TGT GCG ACA GGG GCA GT-3′ (Takahashi and Yamanaka, 2006); *c-Myc* (Tg), 5′-CAC CAT GCC CCT CAA CGT GAA CTT CAC C-3′ and 5′-TTA TGC ACC AGA GTT TCG AAG CTG TTC G-3′ (Takahashi and Yamanaka, 2006); *Klf4* (Tg), 5′-CAC CAT GGC TGT CAG CGA CGC TCT GCT C-3′ and 5′-ACA TCC ACT ACG TGG GAT TTA AAA-3′ (Takahashi and Yamanaka, 2006).

Real-time quantitative RT-PCR analysis

Forward and reverse primers for *Rex1* and *Flk-1* and the fluorogenic probes were designed according to PerkinElmer guidelines (Primer Express Software; PerkinElmer Life and Analytical Sciences, Boston, MA, http://www.perkinelmer.com), and those of *Brachyury* and *Scl* were described in a previous report (Nakanishi et al., 2009; Redmond et al., 2008). The *GAPDH* primers and probes were purchased from Applied Biosystems (Foster City, CA, http://www.appliedbiosystems.com). Quantitative RT-PCR experiments were performed using the ABI-Prism 7300 system (Applied Biosystems) following the manufacturer's instructions. Quantitative assessment of mRNA expression was performed using a GAPDH internal standard. The expression of each mRNA was compared with each day 0 mRNA expression.

The oligonucleotide primers were as follows: mouse *Rex1*, 5′-AAG CAG GAT CGC CTC ACT GT-3′ and 5′-CCG CAA AAA ACT GAT TCT TGG T-3′ (Baba et al., 2007a); mouse *Brachyury*, 5′-TAC CCC AGC CCC TAT GCT CA-3′ and 5′-GGC ACT CCG AGG CTA GAC CA-3′ (Nakanishi et al., 2009); mouse *Scl*, 5′-CAC TAG GCA GTG GGT TCT TTG-3′ and 5′-GGT GTG AGG ACC ATC AGA AAT CT-3′ (Redmond et al., 2008); mouse Flk-1, 5′-AAG CAG GAT CGC CTC ACT GT-3′ and 5′-CCG CAA AAA ACT GAT TCT TGG T-3′ (Baba et al., 2007a).

Colony-forming assay

Every other day of culture, from days 5 through 15, the adherent cells were treated with 0.25% trypsin/EDTA and harvested. They were incubated in a new tissue-culture dish (Becton–Dickinson) for 30 min to eliminate adherent OP9 cells (Suwabe et al., 1998). Floating cells were then collected and cultured at a concentration of 1×10^4 cells/ml in semi-solid α-MEM supplemented with 1.3% methylcellulose, 30% FCS, 10% bovine serum albumin, 100 μM 2ME, and a mixture of the following growth factors: 10 ng/ml human granulocyte colony-stimulating factor (hG-CSF), 2 U/ml hEPO, 20 ng/ml mIL3, 100 ng/ml mSCF, 100 ng/ml hIL6, and 10 ng/ml hTPO. Colony types were determined according to the criteria described previously (Nakahata and Ogawa, 1982a,b,c) by in situ observation using an inverted microscope. The abbreviations used for the clonogenic progenitor cells were as follows: CFU-Mix, mixed colony-forming units; BFU-E, erythroid burst-forming units; CFU-GM, granulocyte–macrophage colony-forming units; and CFU-G, granulocyte colony-forming units.

Single-cell deposition assay

The single-cell deposition assay was performed as described previously (Nishikawa et al., 1998; Umeda et al., 2006; Shinoda et al., 2007). In brief, single sorted cells were deposited in individual wells of 96-well plates with confluent OP9 layers, and cultured for 5 days in the medium described in the "Differentiation of iPS and ES Cells" Section. Each well was stained with a mixture of anti-CD45, CD41, and Ter119 rat antibodies for hematopoietic lineage detection or anti-VE-cadherin rat-antibodies for endothelial lineage detection, respectively. HRP-conjugated goat anti-rat antibodies (Jackson ImmunoResearch Laboratories, Inc.) were used as secondary antibodies.

Statistics

Statistical analyses were conducted using the Student's *t*-test or the Fisher's exact test. Statistical significance was defined as $P < 0.05$.

Results

iPS cells differentiate into hematopoietic cells in coculture with OP9 stromal cells

We initially compared iPS and ES cells by microscopic examination and FACS analysis. The Nanog-iPS cell lines (Okita

et al., 2007) (20D17, 38C2, and 38D2) were positive for green fluorescent protein (GFP) expression only when Nanog was activated. 256H18, which was established by introducing only Oct3/4, Sox2, and Klf4, expressed DsRed (Nakagawa et al., 2008) constitutively. The pMx-GFP retrovirus was introduced into this clone as a silencing indicator. The control D3 ES cells were constitutively positive for GFP. All four of the iPS clones formed ES-like colonies over more than 15 passages (Fig. 1A). The FACS analysis revealed that all of the clones expressed SSEA1, E-cadherin, and CD31 (Fig. 1B), thus demonstrating the phenotypic similarity between iPS and ES cells.

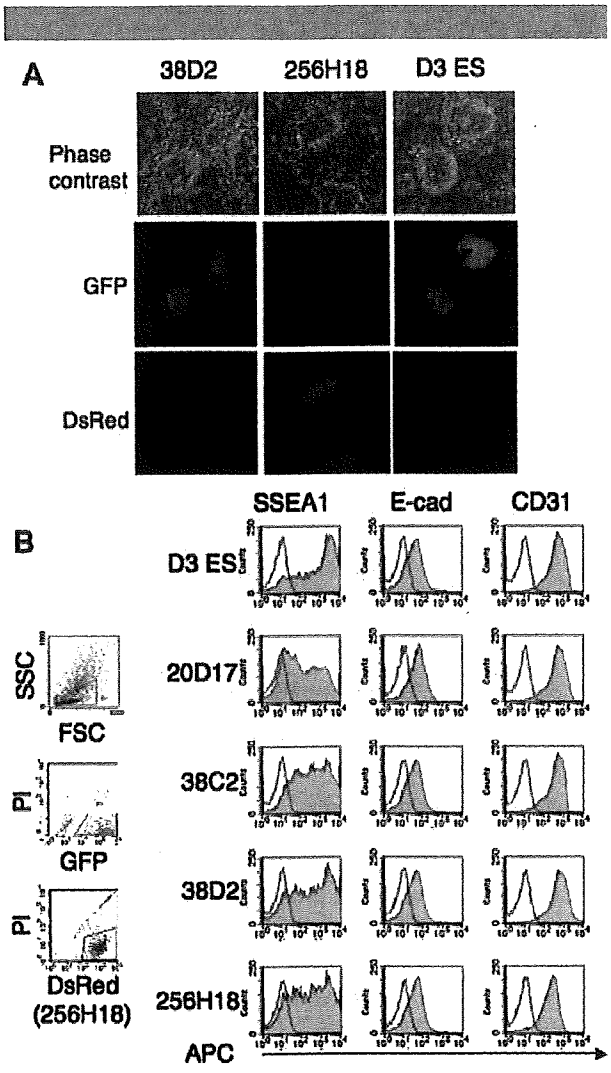

Fig. 1. Formation of ES-like colonies from iPS cells. A: Phase contrast (top row) and fluorescence (middle row: GFP, bottom row: DsRed) micrographs of Nanog-iPS cells (38D2), three-factor (without Myc) iPS (256H18) cells, and D3 ES cells maintained on SNL feeder cells. The D3 ES cells were derived from GFP$^+$ mice. Nanog-iPS cells express GFP only in the undifferentiated state. The three-factor iPS cells were derived from DsRed$^+$ mice, with additional infection by the pMx-GFP virus as a silencing marker. B: FACS analysis showing the phenotypic similarity of iPS and ES cells. The left parts show the gates for eliminating dead cells and contaminated feeders. GFP$^+$PI$^-$ cells (R2) and DSRed$^+$PI$^-$ cells (R4) were gated as ES- and iPS-derived viable cells, respectively. SSEA1, E-cadherin, and CD31 were positive in all strains (shaded bars). Open bars show staining with isotype control antibodies. Representative results from one of three independent experiments performed are presented.

To analyze the hematopoietic differentiation potential of iPS cells, we adapted the OP9 coculture system originally reported by Nakano et al. (1994, 1996). We cocultured iPS cells with OP9 stromal cells for 5 days and transferred the entire culture onto fresh OP9 layers in the presence of mSCF, mIL3, hTPO, and hEPO. Small, round cell colonies first appeared 2 days later (on day 7; Fig. 2A). These colonies gradually grew in both size and number, and a few exhibited areas with a cobblestone-like appearance. Floating cells also appeared on day 7 and thereafter. May–Giemsa staining of the floating cells on day 15 revealed enucleated red blood cells, macrophages, granulocytes, and megakaryocytes (Fig. 2B). The presence of granulocytes and megakaryocytes was confirmed by MPO and acetylcholine esterase (Maherali et al., 2007) staining, respectively. FACS analysis on day 15 confirmed the existence of various types of blood cells, including erythoid and myeloid lineage cells, but not of lymphoid lineage cells (Fig. 2C). These above results demonstrate that iPS cells, like ES cells, can produce hematopoietic cells of various lineages in vitro.

Efficient production of hematopoietic cells from sorted Flk-1$^+$ cells

To thoroughly investigate iPS cell-derived hematopoietic development, we analyzed the expression of Flk-1, a marker of hemoangiogenic progenitors. Although the proportion of Flk-1$^+$ cells in the iPS clones on day 5 varied between 20 ± 2% and 48 ± 9% (Fig. 3A), the temporal patterns of expression were similar in iPS and ES cells. No Flk-1$^+$ cells were detected at

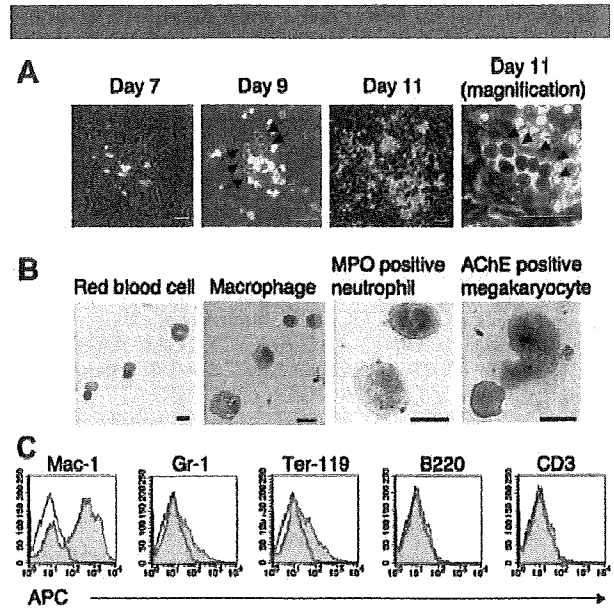

Fig. 2. Hematopoietic cells develop from iPS cells on OP9 feeders. Data from clone 38D2 are shown as representative of iPS-derived hematopoiesis. A: Small colonies first appeared on day 7 (2 days after Flk1$^+$ sorting) and then grew larger. Dark, round hematopoietic progenitors (indicated by arrows) appeared on days 9 and 11, lying beneath the OP9 layer and presenting cobblestone-like areas. Scale bars, 200 μm (left three parts) and 100 μm (rightmost part). B: Floating cells on day 15 included various lineages of hematopoietic cells; enucleated red blood cells, macrophages, MPO$^+$ neutrophils, and AChE$^+$ megakaryocytes were observed. Scale bars, 50 μm. C: Expression of lineage-specific antigens. Floating cells on day 15 were stained with antibodies against macrophages (Mac-1), granulocytes (Gr-1), erythrocytes (Ter-119), B cells (B220), and T cells (CD3). Expression of each antigen (shaded bars) was analyzed using FACS. Open bars show staining with isotype control antibodies.

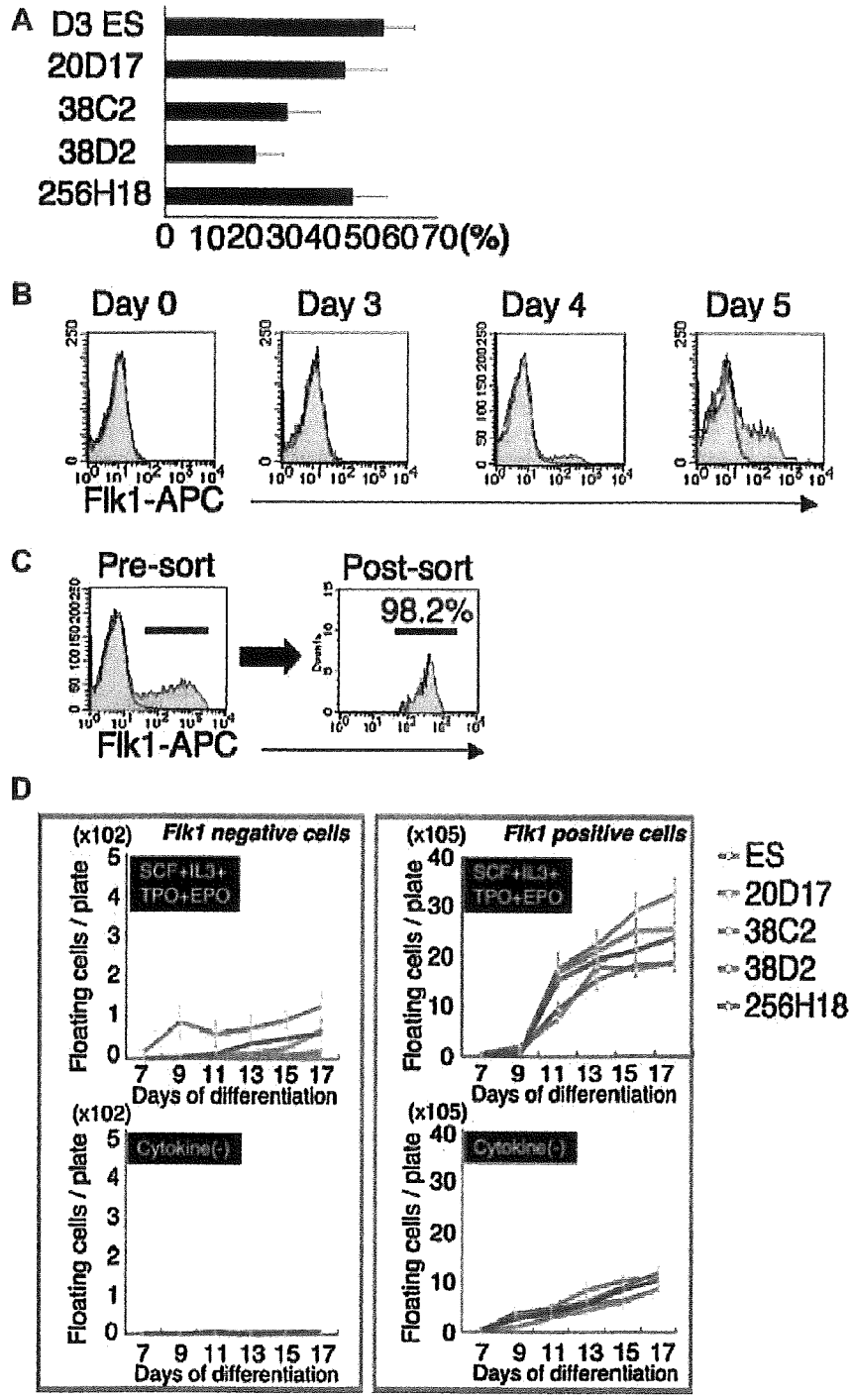

Fig. 3. Efficient production of hematopoietic cells from Flk-1$^+$ populations. A: The amounts of Flk-1$^+$ cells generated from ES and iPS cells at day 5 of differentiation were analyzed by FACS after eliminating OP9 stromal cells as described in Materials and Methods Section. Data are shown as a percentage in the total ES- and iPS-derived viable cells. B: Sequential FACS analysis reveals the emergence of Flk-1$^+$ population after day 4 of differentiation (shaded bars). Open bars show staining with isotype control antibodies. C: Purification of Flk-1$^+$ fractions by FACS on day 5. Reanalysis of the sorted cells confirmed the purity as 93.0–98.2%. D: Sequential analysis of the number of floating cells from ES and iPS cells after sorting with Flk-1 antibody. Sorted Flk-1$^+$ and Flk-1 cells were cultured in the presence or absence of SCF, IL-3, TPO, and EPO. In (A) and (D), data are presented as mean ± SE of three independent duplicate experiments. In (B) and (C), representative data from clone 38D2 are shown.

the outset, but they appeared on day 4 of culture and increased in number until day 5 (Fig. 3B).

We next sorted the Flk-1$^+$ cells on day 5 and cocultured them with fresh OP9 cells. Reanalysis of the sorted Flk-1$^+$ cells by FACS showed that their purity ranged from 93.0% to 98.2% (Fig. 3C). Regardless of the percentage of Flk1$^+$ cells before sorting, all of the iPS cell lines and ES cells could produce similar yields of hematopoietic cells predominantly from Flk-1$^+$ fractions, and exogenous cytokines increased the hematopoietic efficacy fourfold (Fig. 3D).

Primitive and definitive hematopoietic development of iPS cells

In the developing mouse embryo, primitive hematopoiesis originates in the extra-embryonic yolk sac on day 7.5 of gestation (Moore and Metcalf, 1970). Thereafter, definitive hematopoiesis emerges as a second wave in the aorta-gonad-mesonephros (AGM) region and replaces primitive hematopoiesis (Muller et al., 1994; Medvinsky and Dzierzak, 1996; Matsuoka et al., 2001). Primitive and definitive erythrocytes are morphologically distinguishable, and show distinct patterns of hemoglobin gene expression: the former are larger, nucleated cells that express not only embryonic ε-globin and ζ-globin but also adult α-globin, whereas the latter are smaller, enucleated cells expressing only adult α-globin and β-globin (Doetschman et al., 1985; Leder et al., 1992; Nakano et al., 1996; Xu et al., 2001).

To investigate whether primitive and definitive erythropoiesis can occur in iPS cells, we initially examined floating hematopoietic cells (Fig. 4A). May–Giemsa staining revealed that on day 7 the cells were large and nucleated, resembling primitive erythrocytes, whereas on day 15 they were smaller, enucleating or enucleated, and similar to definitive erythrocytes. Immunostaining revealed that day 7 cells were strongly positive for embryonic hemoglobin but negative for β-major hemoglobin, while day 15 cells expressed β-major hemoglobin strongly, with little or no expression of embryonic hemoglobin.

We also examined globin gene expression in the floating cells by sequential RT-PCR (Fig. 4B). The expressions of ε-globin and ζ-globin were strongest on day 7, decreased thereafter until day 11, and were undetectable on days 13–17. In contrast, α-globin and β-major globin expression were observed from days 9 through 17. These expression patterns were similar in iPS and ES cells, suggesting that iPS cells in vitro, like ES cells, can undergo primitive followed by definitive erythropoiesis.

Hematopoietic stem/progenitor cells develop from iPS-derived Flk-1$^+$ cells

To verify the formation of hematopoietic stem/progenitor cells in our culture system, we initially examined the expressions of c-kit, Sca1, CD34, and CD45, which are expressed by early hematopoietic progenitors (van de Rijn et al., 1989; Motro et al., 1991; Ling and Neben, 1997). FACS analysis revealed that undifferentiated iPS and ES cells expressed c-kit and Sca1, but not CD34 or CD45. Subsequent examination revealed the transient downregulation of Sca1 and c-kit on day 3, with Sca1 expression increasing again on day 5. On day 13 (8 days after cell sorting), we detected a new cell population that was positive for c-kit, Sca1, CD34, and CD45 (Fig. 5A,B).

We next investigated whether clonogenic hematopoietic cells were also produced in our culture system. Methylcellulose colony-forming assays showed that CFU-Mix, BFU-E, CFU-GM, and CFU-G colonies, as described in Materials and Methods Section, developed from the iPS-derived cells (Fig. 5C), and their numbers were not much lower than those formed by ES-derived cells (Fig. 5D). CFU-Mix and BFU-E colonies predominated the Flk-1$^+$ cells on days 7 and 9, but then

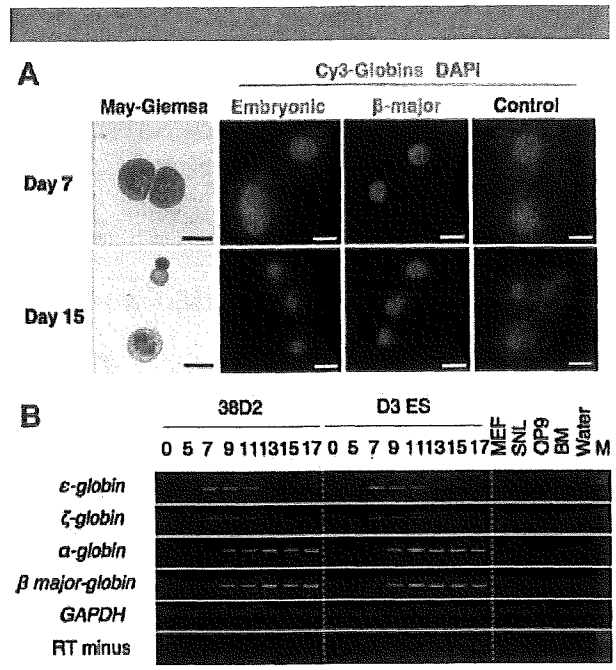

Fig. 4. Primitive and definitive erythrocytes formed from iPS cells. A: iPS-derived floating hematopoietic cells on day 7 (upper row) and day 15 (lower row) are shown. Erythrocytes on day 7 were larger and nucleated, and strongly positive for embryonic hemoglobin, but negative for β-major globin. Red blood cells on day 15 were smaller and enucleating or enucleated, and positive for β-major globin. B: Sequential RT-PCR analysis of globin gene expressions. RNA was isolated from all cells during the initiation culture (days 0 and 5), and from floating cells during the hematopoietic culture (day 7 and thereafter). GAPDH was used as a loading control. MEF, murine embryonic fibroblasts; SNL, SNL feeder cells; OP9, OP9 feeder cells; BM, adult murine bone marrow; M, 200-bp size marker. Representative results are shown from one of three independent experiments performed on clone 38D2.

decreased; the majority of cells after day 11 were from the CFU-GM and CFU-G colonies. These results suggest that iPS cells can generate multipotent hematopoietic progenitors almost as efficiently as ES cells.

Concomitant development of endothelial cells from iPS-derived Flk-1$^+$ cells

We next evaluated the development of endothelial lineages in our system. At 5 days after sorting, sheet-like colonies appeared that took up Dil-acetylated low-density lipoprotein (Dil-Ac-LDL) and were positive for anti-endothelial nitric oxide synthase (eNOS), CD31, and VE-cadherin (Fig. 6A). As shown in Figure 6B, iPS-derived Flk-1$^+$ cells produced many more VE-cadherin$^+$ colonies than Flk-1$^-$ cells ($P < 0.05$).

We also analyzed the expression of the following genes that are associated with the development of hematopoietic and endothelial lineages (Fig. 6C): required for excision 1 (*Rex1*; undifferentiated cells), *Brachyury* (primitive streak and mesoderm), *Flk-1* (mesoderm), GATA-binding protein 2 (*GATA2*; hematopoietic and endothelial), *SCL* (hematopoietic), *Myb* (hematopoietic), *GATA1* (hematopoietic), and tyrosine kinase with Ig-like and endothelial growth factor-like domains 1 (*Tie1*; endothelial). Both ES and iPS cells expressed *Rex1* strongly in the undifferentiated state. *Rex1* expression gradually decreased during differentiation, and *Brachyury*, *Flk-1*, and *SCL* expressions initially appeared on day 3. Quantitative real-time PCR analyses confirmed that *Brachyury* expression increased to

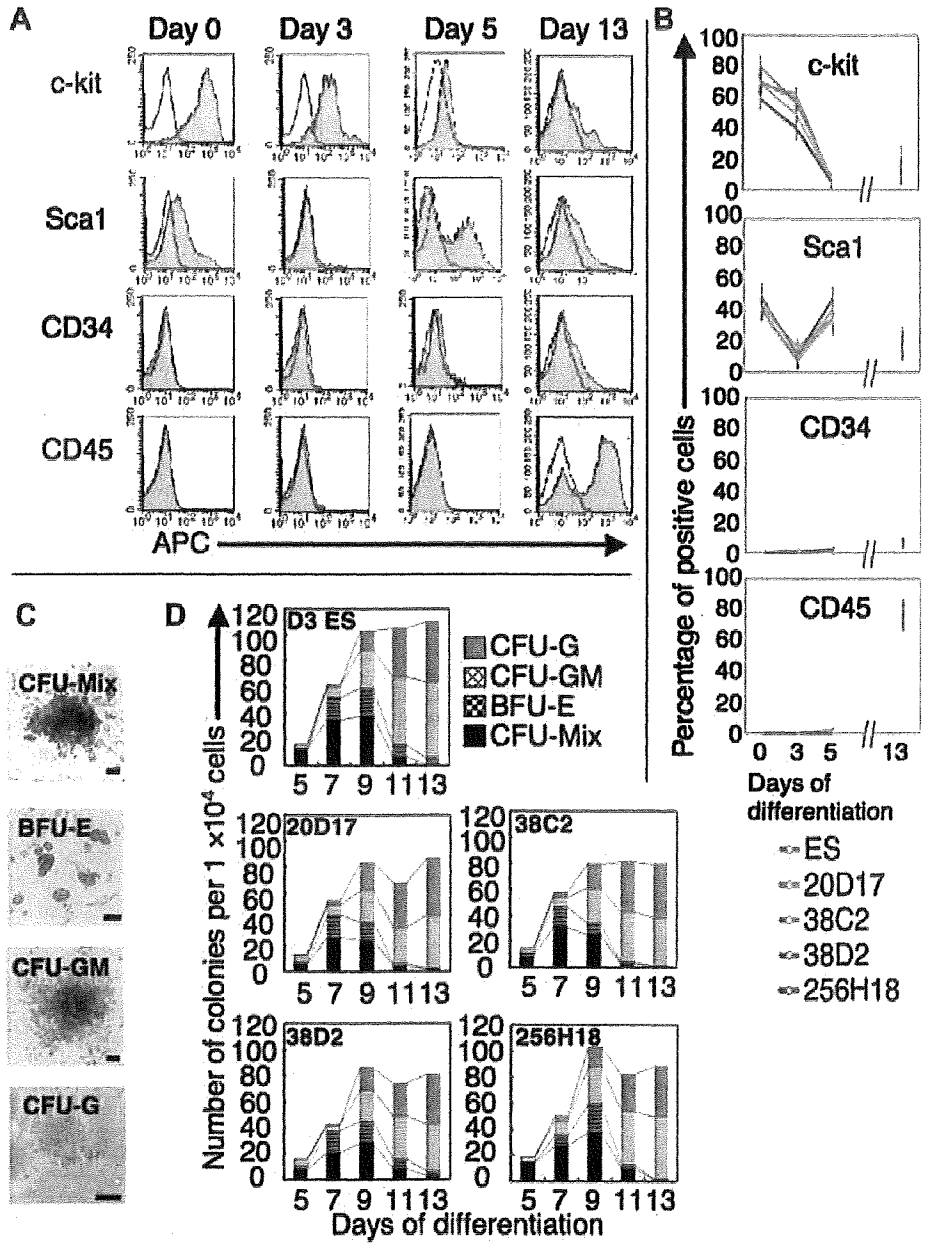

Fig. 5. Hematopoietic stem/progenitor cells emerge from Flk-1$^+$ cells. Sequential FACS analysis of c-kit, Sca1, CD34, and CD45 in ES and iPS-derived cells during differentiation. Whole culture were harvested on indicated days and analyzed by FACS as described in Materials and Methods Section. A: Representative data from clone 38D2 are shown. Histograms show the isotype control staining profile (open bars) versus the specific antibody staining profiles (shaded bars). B: Percentages of each antigen positive cells generated from ES and iPS cells are presented as mean ± SE of three independent duplicate experiments. C: The iPS cells formed various colony types on MTC-containing medium. Data from clone 38D2 are shown as representative. Scale bars, 200 μm. D: Numbers of each colony type derived from ES and iPS cells. Data represent mean of three independent triplicate experiments.

a maximum on day 3, followed by the upregulation of *Flk-1* and *SCL* (Fig. 6D). *Brachyury* expression continued until day 7, whereas that of *Flk-1* and *SCL* could be detected until day 9. *GATA2*, *Myb*, *GATA1*, and *Tie1* expressions were initially detected on day 5, and persisted thereafter. Taken together, these results demonstrate that, in our system, hematopoietic and/or endothelial differentiation of iPS cells occurs in a similar manner to that observed during embryogenesis.

Common hemoangiogenic progenitors are present in iPS-derived Flk-1$^+$ populations

Previous work has demonstrated that common hemoangiogenic progenitors are present in Flk-1$^+$ cells during ES-cell differentiation (Nishikawa et al., 1998). To investigate whether iPS-derived Flk-1$^+$ cells possess the same differentiation potential, we performed a single-cell deposition

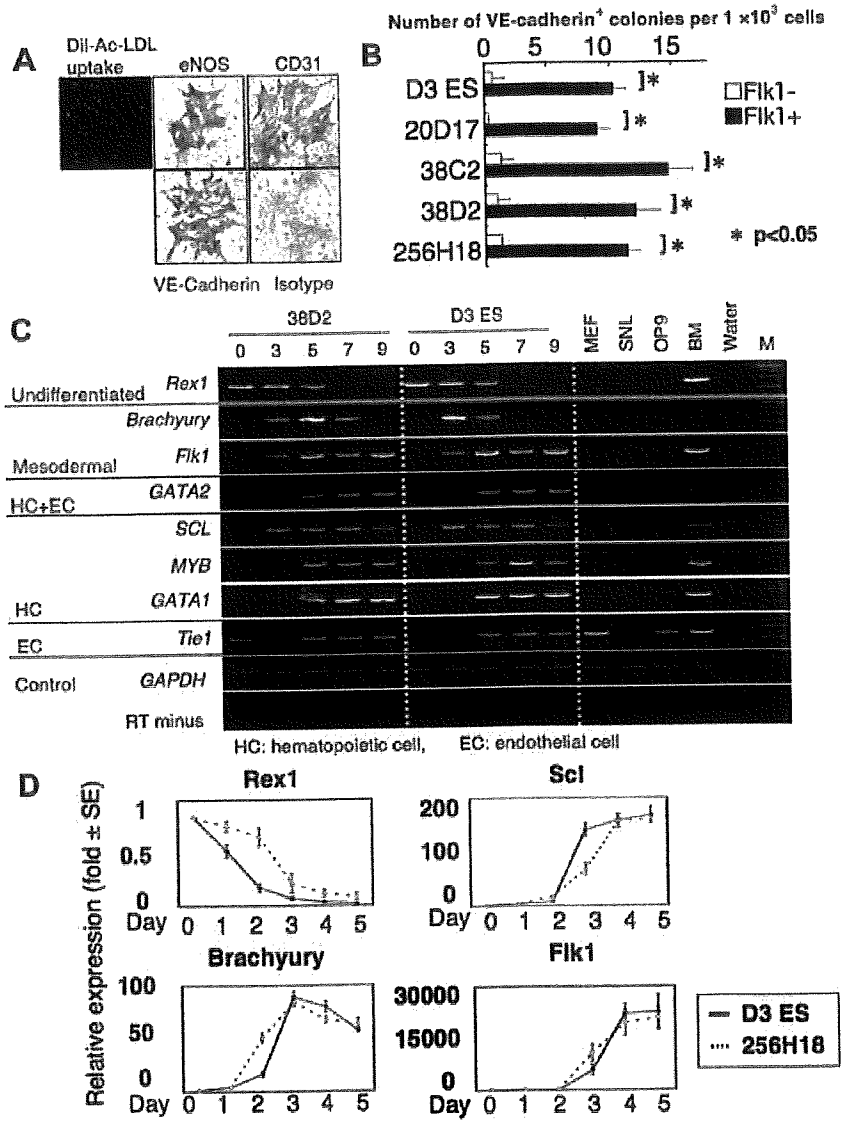

Fig. 6. Concomitant endothelial and hematopoietic development from iPS-derived Flk-1$^+$ cells. A: The sheet-like colonies took up Dil-Ac-LDL and were positive for eNOS, CD31, and VE-cadherin. Data from clone 38D2 are shown as representative. B: Number of VE-cadherin$^+$ colonies per 1×10^3 Flk1$^+$ or Flk1$^-$ cells derived from ES and iPS cells. Data are presented as mean ± SD of three independent experiments. C: RT-PCR using mRNA isolated from ES and iPS-derived cells during culture. HC and EC means hematopoietic and endothelial cells, respectively. GAPDH was used as a loading control. M: 200 bp size marker. Representative results from one of three independent experiments performed on clone 38D2 are shown. D: The expressions of *Rex1*, *Brachyury*, *Scl*, and *Flk-1* were evaluated by real-time quantitative RT-PCR. mRNA samples were harvested from D3 ES-derived GFP$^+$ cells or clone 256H18-derived DsRed$^+$ cells sorted by FACS on indicated days. Values were normalized to *gapdh* mRNA, and the control values were arbitrarily set to day 0 (undifferentiated ES cells). Data represent the mean ± SE of three independent duplicate experiments.

assay using the DsRed$^+$ clone 256H18. Single Flk-1$^+$ cells were deposited in four 96-well culture dishes (384 wells) containing OP9 feeder cells. Each well was observed by fluorescence microscopy 24 h after cell deposition, and wells that contained more than one DsRed$^+$ cell were excluded from further analysis. The presence of hematopoietic (Woodard et al., 2000) and endothelial (Maherali et al., 2007) colonies was confirmed not only morphologically, but also by immunostaining with a mixture of anti-CD41, CD45, and Ter119 antibodies, and anti-VE-cadherin antibodies, respectively, as previously reported (Fig. 7A) (Nishikawa et al., 1998). After 5 days of culture, the clonal outgrowth rates were 10.2% and 8.9% from 256H18 iPS and D3 ES cells, respectively. The frequencies of EC development alone, HC development alone, and HC plus EC development, respectively, were 2.7%, 5.2%, and 2.2%, respectively, from iPS cells and 2.4%, 3.5%, and 2.9%, respectively, from ES cells (Fig. 7B). Thus, the potential for mono- or bipotential progenitor development from iPS cells was almost equivalent to that from ES cells.

Discussion

Induced PS cells may serve as a novel cell source in both research and the clinic because, like ES cells, they have an

A

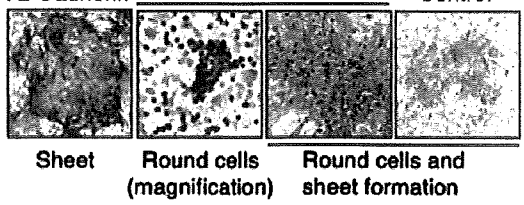

B

Clones	Only one cell 24 hours after sorting	After 5 days		
		HC	EC	HC+EC
DsRed iPS cells (256H18)	361 wells	10 wells (2.7%)	19 wells (5.2%)	8 wells (2.2%)
D3 ES cells	369 wells	9 wells (2.4%)	13 wells (3.5%)	11 wells (2.9%)

HC: Hematopoietic cells
EC: Endothelial cells

Fig. 7. Common hemoangiogenic progenitors are present in Flk-1$^+$ cells during iPS-cell differentiation. A: Single Flk-1$^+$ cells were cultured on OP9 layers in the wells of 96-well plates and immunostained with anti-VE-cadherin antibodies, or a cocktail of anti-CD41, anti-CD45, and anti-Ter119 antibodies, 7 days after sorting. B: Number of wells that showed EC (endothelial cells), HC (hematopoietic cells), and EC + HC development were counted as described in text.

unlimited capacity for self-renewal (Takahashi and Yamanaka, 2006; Meissner et al., 2007; Okita et al., 2007; Park et al., 2007; Takahashi et al., 2007; Yu et al., 2007; Aoi et al., 2008; Hanna et al., 2008; Nakagawa et al., 2008). The use of customized pluripotent stem cells would avoid the controversies surrounding ES cells. A recent study demonstrated that, after additional genetic manipulation and hematopoietic stem/progenitor cell expansion, autologous iPS cells could be used to treat mice with sickle-cell anemia, clearly revealing the advantage of these cells in regenerative medicine (Hanna et al., 2007).

One significant advantage of iPS cells is that cells from each patient can be used to screen drugs or to examine the effects of novel procedures against various diseases. Many diseases have a complex genetic etiology that affects the development, differentiation, and maturation of different tissues and organs, and require an experimental model system to faithfully reproduce their altered developmental processes (Lensch and Daley, 2006). In light of the heterogeneity of disease phenotypes and drug toxicity, it is desirable to establish defined sources of cells for drug discovery and research. In this area, immortalized cell lines and tissue-specific stem/progenitor cells that have been used for such studies are now being replaced by pluripotent stem cells.

The present study demonstrates that murine iPS cells can recapitulate early hematopoietic development in vitro. We confirmed the step-wise development of primitive and definitive hematopoietic cells, as well as endothelial cells, from Flk-1$^+$ hemoangiogenic progenitors, together with the upregulation of genes related to both lineages. Both lineages could be generated from individual Flk-1$^+$ cells, strongly suggesting the existence of common progenitor "hemangioblasts," as was previously reported for ES cells and embryos (Flamme et al., 1995; Risau, 1995; Risau and Flamme, 1995; Choi et al., 1998; Huber et al., 2004).

Step-wise development of primitive and definitive hematopoiesis from iPS-derived intermediate mesodermal progenitors

During embryogenesis, primitive hematopoiesis emerges in the yolk sac on 7.5 d.p.c. Following this process, definitive hematopoiesis, which is the major hematopoietic process throughout life, originates on 8.5 d.p.c. in the AGM region (Muller et al., 1994; Medvinsky and Dzierzak, 1996; Matsuoka et al., 2001). When the site of hematopoiesis shifts to the fetal liver on 10.5 d.p.c. and finally to the bone marrow, the number of blood cells massively increases; erythroid cell lineages are the major products in the fetal liver, and myeloid lineages appear at later stages. Here we demonstrated that Flk-1$^+$ mesodermal cells derived from iPS cells can lead to both primitive and definitive hematopoiesis.

Interestingly, the time courses of the hematopoietic differentiation of iPS and ES cell lines in our experiments were almost precisely synchronized with those seen in embryonic development. Hematopoietic colonies on the OP9 layer were first observed on day 7 of differentiation, and the number of cells produced increased explosively from day 11. Immunostaining and RT-PCR indicated a shift from primitive to definitive hematopoiesis as differentiation progressed over time. Moreover, the results of the MTC colony-forming assay also suggested that hematopoietic differentiation in our system reflects that occurring in embryogenesis: CFU-Mix and BFU-E colonies were mainly observed until day 9, while CFU-GM and CFU-G colonies became dominant on day 11 and thereafter.

Identifying and inducing hematopoietic stem cells (HSCs) in vitro is of great biological interest. Previous studies have suggested that the cobblestone area forming cells (CAFCs) observed in the OP9 system are indicative of the existence of primitive hematopoietic progenitors (Suwabe et al., 1998); CD34, c-kit, and Sca1 are among the characteristic markers of HSCs or very immature progenitors. In our study, we observed CAFCs derived from iPS cells, and FACS analyses revealed that many of the iPS-derived hematopoietic cells expressed the progenitor markers mentioned above. Taken together, these findings suggest that iPS cells can produce very immature hematopoietic progenitors in vitro. In the future, further study will be necessary to investigate whether iPS cells can generate true HSCs that demonstrate long-term multilineage marrow reconstitution in lethally irradiated mice without any additional gene manipulation.

Concomitant differentiation of iPS cells into hematopoietic and endothelial lineages

Several in vivo and in vitro studies have demonstrated a close association between hematopoietic and endothelial differentiation. Previous experiments have shown that murine and primate ES cells differentiate into hematopoietic cells via common Flk1$^+$ hemoangiogenic progenitors (Nishikawa et al., 1998; Umeda et al., 2006). Using RT-PCR and the single-cell deposition assay, our study demonstrated that iPS cells, like ES cells, can generate hematopietic and endothelial cells concomitantly, as is observed in embryogenesis.

The RT-PCR data demonstrated that the expression of the early mesodermal marker *Brachyury* was followed by that of *flk-1* and *scl*, both of which are crucial for the development of common progenitors (Nishikawa et al., 1998; Chung et al., 2002). The expression of genes associated with both lineages began thereafter. These results suggest that the orchestrated process from mesoderm development to the specification of either lineage during embryogenesis is also recapitulated in the iPS-cell model.

The single-deposition assay demonstrated that iPS cells possess an equivalent capacity to ES cells to develop bipotent progenitors at the single cell level. However, the frequency of progenitor development was unexpectedly low. One possible reason for this is the low clonal growth rate in our single-cell culture condition. Another possibility is that the sorted Flk-1$^+$ cells included, besides hemangioblasts, progenitors that contribute to other mesodermal lineages. Recent studies on murine ES and iPS cells demonstrated the development of cardiac muscles, vascular smooth muscles, and pericytes from Flk-1$^+$ fractions (Yamashita et al., 2000; Iida et al., 2005; Baba et al., 2007b; Narazaki et al., 2008). We also observed the formation of contractile colonies from Flk-1$^+$ fractions (data not shown). This may be one alternative reason for the observed low frequency of differentiation of either lineage. Further studies will enhance our understanding of the developmental biology of iPS cells.

Hematopoietic potential of iPS-derived Flk-1$^+$ progenitors is equivalent, regardless of the clone

In our experiments, the efficacy of Flk-1$^+$ cell induction varied between the clones, although the timing of their differentiation was the same. This may be potentially due to contamination by the SNL feeder cells. As these feeder cells were not eliminated at the start of differentiation, they would have remained throughout the assay and might have inhibited differentiation. However, to address these problems, it will be necessary to study the biological characteristics of iPS cells further, including their epigenetic behavior during differentiation. The most interesting and encouraging finding in our study was that the sorted Flk-1$^+$ cells derived from all analyzed iPS and ES clones were similar in their ability to generate hematopoietic cells.

In conclusion, our results demonstrate that iPS cells can develop into hematopoietic cells in vitro via hemoangiogenic progenitors, the so-called "hemangioblasts." Furthermore, iPS cells traverse the primitive and definitive hematopoietic stages in a manner similar to that observed during embryogenesis. Although future investigations at the biological and molecular levels are highly desirable, our study suggests that iPS cells hold great promise in medicine, and may aid in attaining the long sought goal of patient-specific stem cells.

Acknowledgments

This work was supported by grants from the Ministry of Education, Culture, Sports, Science, and Technology of Japan.

Literature Cited

Aoi T, Yae K, Nakagawa M, Ichisaka T, Okita K, Takahashi K, Chiba T, Yamanaka S. 2008. Generation of pluripotent stem cells from adult mouse liver and stomach cells. Science (New York, NY) 321:699–702.

Baba S, Heike T, Umeda K, Iwasa T, Kaichi S, Hiraumi Y, Doi H, Yoshimoto M, Kanatsu-Shinohara M, Shinohara T, Nakahata T. 2007a. Generation of cardiac and endothelial cells from neonatal mouse testis-derived multipotent germline stem cells. Stem Cells (Dayton, Ohio) 25:1375–1383.

Baba S, Heike T, Yoshimoto M, Umeda K, Doi H, Iwasa T, Lin X, Matsuoka S, Komeda M, Nakahata T. 2007b. Flk1(+) cardiac stem/progenitor cells derived from embryonic stem cells improve cardiac function in a dilated cardiomyopathy mouse model. Cardiovasc Res 76:119–131.

Choi K, Kennedy M, Kazarov A, Papadimitriou JC, Keller G. 1998. A common precursor for hematopoietic and endothelial cells. Development (Cambridge, England) 125:725–732.

Chung YS, Zhang WJ, Arentson E, Kingsley PD, Palis J, Choi K. 2002. Lineage analysis of the hemangioblast as defined by FLK1 and SCL expression. Development (Cambridge, England) 129:5511–5520.

Doetschman TC, Eistetter H, Katz M, Schmidt W, Kemler R. 1985. The in vitro development of blastocyst-derived embryonic stem cell lines: Formation of visceral yolk sac, blood islands and myocardium. J Embryol Exp Morphol 87:27–45.

Evans MJ, Kaufman MH. 1981. Establishment in culture of pluripotential cells from mouse embryos. Nature 292:154–156.

Flamme I, Breier G, Risau W. 1995. Vascular endothelial growth factor (VEGF) and VEGF receptor 2 (flk-1) are expressed during vasculogenesis and vascular differentiation in the quail embryo. Dev Biol 169:699–712.

Garcia-Porrero JA, Manaia A, Jimeno J, Lasky LL, Dieterlen-Lievre F, Godin IE. 1998. Antigenic profiles of endothelial and hemopoietic lineages in murine intraembryonic hemogenic sites. Dev Comp Immunol 22:303–319.

Hanna J, Wernig M, Markoulaki S, Sun CW, Meissner A, Cassady JP, Beard C, Brambrink T, Wu LC, Townes TM, Jaenisch R. 2007. Treatment of sickle cell anemia mouse model with iPS cells generated from autologous skin. Science (New York, NY) 318:1920–1923.

Hanna J, Markoulaki S, Schorderet P, Carey BW, Beard C, Wernig M, Creyghton MP, Steine EJ, Cassady JP, Foreman R, Lengner CJ, Dausman JA, Jaenisch R. 2008. Direct reprogramming of terminally differentiated mature B lymphocytes to pluripotency. Cell 133:250–264.

Hansen JN, Konkel DA, Leder P. 1982. The sequence of a mouse embryonic beta-globin gene. Evolution of the gene and its signal region. J Biol Chem 257:1048–1052.

Huber TL, Kouskoff V, Fehling HJ, Palis J, Keller G. 2004. Haemangioblast commitment is initiated in the primitive streak of the mouse embryo. Nature 432:625–630.

Iida M, Heike T, Yoshimoto M, Baba S, Doi H, Nakahata T. 2005. Identification of cardiac stem cells with FLK1, CD31, and VE-cadherin expression during embryonic stem cell differentiation. FASEB J 19:371–378.

Jackson CW. 1973. Cholinesterase as a possible marker for early cells of the megakaryocytic series. Blood 42:413–421.

Jaenisch R, Young R. 2008. Stem cells, the molecular circuitry of pluripotency and nuclear reprogramming. Cell 132:567–582.

Konkel DA, Tilghman SM, Leder P. 1978. The sequence of the chromosomal mouse beta-globin major gene: Homologies in capping, splicing and poly(A) sites. Cell 15:1125–1132.

Ku HT, Zhang N, Kubo A, O'Connor R, Mao M, Keller G, Bromberg JS. 2004. Committing embryonic stem cells to early endocrine pancreas in vitro. Stem Cells (Dayton, Ohio) 22:1205–1217.

Kyba M, Perlingeiro RC, Daley GQ. 2002. HoxB4 confers definitive lymphoid-myeloid engraftment potential on embryonic stem cell and yolk sac hematopoietic progenitors. Cell 109:29–37.

Kyba M, Perlingeiro RC, Hoover RR, Lu CW, Pierce J, Daley GQ. 2003. Enhanced hematopoietic differentiation of embryonic stem cells conditionally expressing Stat5. Proc Natl Acad Sci USA 100:11904–11910.

Leder A, Weir L, Leder P. 1985. Characterization, expression, and evolution of the mouse embryonic zeta-globin gene. Mol Cell Biol 5:1025–1033.

Leder A, Kuo A, Shen MM, Leder P. 1992. In situ hybridization reveals co-expression of embryonic and adult alpha globin genes in the earliest murine erythrocyte progenitors. Development (Cambridge, England) 116:1041–1049.

Lensch MW, Daley GQ. 2006. Scientific and clinical opportunities for modeling blood disorders with embryonic stem cells. Blood 107:2605–2612.

Ling V, Neben S. 1997. In vitro differentiation of embryonic stem cells: Immunophenotypic analysis of cultured embryoid bodies. J Cell Physiol 171:104–115.

Maherali N, Sridharan R, Xie W, Utikal J, Eminli S, Arnold K, Stadtfeld M, Yachechko R, Tchieu J, Jaenisch R, Plath K, Hochedlinger K. 2007. Directly reprogrammed fibroblasts show global epigenetic remodeling and widespread tissue contribution. Cell Stem Cell 1:55–70.

Matsuoka S, Tsuji K, Hisakawa H, Xu M, Ebihara Y, Ishii T, Sugiyama D, Manabe A, Tanaka R, Ikeda Y, Asano S, Nakahata T. 2001. Generation of definitive hematopoietic stem cells from murine early yolk sac and paraaortic splanchnopleures by aorta-gonad-mesonephros region-derived stromal cells. Blood 98:6–12.

Medvinsky A, Dzierzak E. 1996. Definitive hematopoiesis is autonomously initiated by the AGM region. Cell 86:897–906.

Meissner A, Wernig M, Jaenisch R. 2007. Direct reprogramming of genetically unmodified fibroblasts into pluripotent stem cells. Nat Biotechnol 25:1177–1181.

Miwa Y, Atsumi T, Imai N, Ikawa Y. 1991. Primitive erythropoiesis of mouse teratocarcinoma stem cells PCC3/A/1 in serum-free medium. Development (Cambridge, England) 111:543–549.

Moore MA, Metcalf D. 1970. Ontogeny of the haemopoietic system: Yolk sac origin of in vivo and in vitro colony forming cells in the developing mouse embryo. Br J Haematol 18:279–296.

Motro B, van der Kooy D, Rossant J, Reith A, Bernstein A. 1991. Contiguous patterns of c-kit and steel expression: Analysis of mutations at the W and Sl loci. Development (Cambridge, England) 113:1207–1221.

Muller AM, Medvinsky A, Strouboulis J, Grosveld F, Dzierzak E. 1994. Development of hematopoietic stem cell activity in the mouse embryo. Immunity 1:291–301.

Nakagawa M, Koyanagi M, Tanabe K, Takahashi K, Ichisaka T, Aoi T, Okita K, Mochiduki Y, Takizawa N, Yamanaka S. 2008. Generation of induced pluripotent stem cells without Myc from mouse and human fibroblasts. Nat Biotechnol 26:101–106.

Nakahata T, Ogawa M. 1982a. Clonal origin of murine hemopoietic colonies with apparent restriction to granuclocyte-macrophage-megakaryocyte (GMM) differentiation. J Cell Physiol 111:239–246.

Nakahata T, Ogawa M. 1982b. Hemopoietic colony-forming cells in umbilical cord blood with extensive capability to generate mono- and multipotential hemopoietic progenitors. J Clin Invest 70:1324–1328.

Nakahata T, Ogawa M. 1982c. Identification in culture of a class of hemopoietic colony-forming units with extensive capability to self-renew and generate multipotential hemopoietic colonies. Proc Natl Acad Sci USA 79:3843–3847.

Nakanishi M, Kurisaki A, Hayashi Y, Warashina M, Ishiura S, Kusuda-Furue M, Asashima M. 2009. Directed induction of anterior and posterior primitive streak by Wnt from embryonic stem cells cultured in a chemically defined serum-free medium. FASEB J 23:114–122.

Nakano T, Kodama H, Honjo T. 1994. Generation of lymphohematopoietic cells from embryonic stem cells in culture. Science (New York, NY) 265:1098–1101.

Nakano T, Kodama H, Honjo T. 1996. In vitro development of primitive and definitive erythrocytes from different precursors. Science (New York, NY) 272:722–724.

Narazaki G, Uosaki H, Teranishi M, Okita K, Kim B, Matsuoka S, Yamanaka S, Yamashita JK. 2008. Directed and systematic differentiation of cardiovascular cells from mouse induced pluripotent stem cells. Circulation 118:498–506.

Nishikawa SI, Nishikawa S, Hirashima M, Matsuyoshi N, Kodama H. 1998. Progressive lineage analysis by cell sorting and culture identifies FLK1+VE-cadherin+ cells at a diverging point of endothelial and hemopoietic lineages. Development (Cambridge, England) 125:1747–1757.

Nishioka Y, Leder P. 1979. The complete sequence of a chromosomal mouse alpha-globin gene reveals elements conserved throughout vertebrate evolution. Cell 18:875–882.

Okita K, Ichisaka T, Yamanaka S. 2007. Generation of germline-competent induced pluripotent stem cells. Nature 448:313–317.

Park IH, Zhao R, West JA, Yabuuchi A, Huo H, Ince TA, Lerou PH, Lensch MW, Daley GQ. 2007. Reprogramming of human somatic cells to pluripotency with defined factors. Nature 451:141–146.

Redmond LC, Dumur CI, Archer KJ, Haar JL, Lloyd JA. 2008. Identification of erythroid-enriched gene expression in the mouse embryonic yolk sac using microdissected cells. Dev Dyn 237:436–446.

Risau W. 1995. Differentiation of endothelium. FASEB J 9:926–933.
Risau W, Flamme I. 1995. Vasculogenesis. Annu Rev Cell Dev Biol 11:73–91.
Shalaby F, Ho J, Stanford WL, Fischer KD, Schuh AC, Schwartz L, Bernstein A, Rossant J. 1997. A requirement for Flk1 in primitive and definitive hematopoiesis and vasculogenesis. Cell 89:981–990.
Shimizu R, Takahashi S, Ohneda K, Engel JD, Yamamoto M. 2001. In vivo requirements for GATA-1 functional domains during primitive and definitive erythropoiesis. EMBO J 20:5250–5260.
Shimizu R, Kuroha T, Ohneda O, Pan X, Ohneda K, Takahashi S, Philipsen S, Yamamoto M. 2004. Leukemogenesis caused by incapacitated GATA-1 function. Mol Cell Biol 24:10814–10825.
Shinoda G, Umeda K, Heike T, Arai M, Niwa A, Ma F, Suemori H, Luo HY, Chui DH, Torii R, Shibuya M, Nakatsuji N, Nakahata T. 2007. alpha4-Integrin(+) endothelium derived from primate embryonic stem cells generates primitive and definitive hematopoietic cells. Blood 109:2406–2415.
Suwabe N, Takahashi S, Nakano T, Yamamoto M. 1998. GATA-1 regulates growth and differentiation of definitive erythroid lineage cells during in vitro ES cell differentiation. Blood 92:4108–4118.
Takahashi K, Yamanaka S. 2006. Induction of pluripotent stem cells from mouse embryonic and adult fibroblast cultures by defined factors. Cell 126:663–676.
Takahashi K, Tanabe K, Ohnuki M, Narita M, Ichisaka T, Tomoda K, Yamanaka S. 2007. Induction of pluripotent stem cells from adult human fibroblasts by defined factors. Cell 131:861–872.
Umeda K, Heike T, Yoshimoto M, Shiota M, Suemori H, Luo HY, Chui DH, Torii R, Shibuya M, Nakatsuji N, Nakahata T. 2004. Development of primitive and definitive hematopoiesis from nonhuman primate embryonic stem cells in vitro. Development (Cambridge, England) 131:1869–1879.
Umeda K, Heike T, Yoshimoto M, Shinoda G, Shiota M, Suemori H, Luo HY, Chui DH, Torii R, Shibuya M, Nakatsuji N, Nakahata T. 2006. Identification and characterization of hemoangiogenic progenitors during cynomolgus monkey embryonic stem cell differentiation. Stem Cells (Dayton, Ohio) 24:1348–1358.
van de Rijn M, Heimfeld S, Spangrude GJ, Weissman IL. 1989. Mouse hematopoietic stem-cell antigen Sca-1 is a member of the Ly-6 antigen family. Proc Natl Acad Sci USA 86:4634–4638.
Vodyanik MA, Slukvin II. 2007. Hematoendothelial differentiation of human embryonic stem cells. Curr Protoc Cell Biol Chapter 23:Unit 23.6.
Vodyanik MA, Bork JA, Thomson JA, Slukvin II. 2005. Human embryonic stem cell-derived CD34+ cells: Efficient production in the coculture with OP9 stromal cells and analysis of lymphohematopoietic potential. Blood 105:617–626.
Wood HB, May G, Healy L, Enver T, Morriss-Kay GM. 1997. CD34 expression patterns during early mouse development are related to modes of blood vessel formation and reveal additional sites of hematopoiesis. Blood 90:2300–2311.
Woodard JP, Gulbahce E, Shreve M, Steiner M, Peters C, Hite S, Ramsay NK, DeFor T, Baker KS. 2000. Pulmonary cytolytic thrombi: A newly recognized complication of stem cell transplantation. Bone Marrow Transplant 25:293–300.
Xu MJ, Matsuoka S, Yang FC, Ebihara Y, Manabe A, Tanaka R, Eguchi M, Asano S, Nakahata T, Tsuji K. 2001. Evidence for the presence of murine primitive megakaryocytopoiesis in the early yolk sac. Blood 97:2016–2022.
Yamashita J, Itoh H, Hirashima M, Ogawa M, Nishikawa S, Yurugi T, Naito M, Nakao K. 2000. Flk1-positive cells derived from embryonic stem cells serve as vascular progenitors. Nature 408:92–96.
Yang FC, Tsuji K, Oda A, Ebihara Y, Xu MJ, Kaneko A, Hanada S, Mitsui T, Kikuchi A, Manabe A, Watanabe S, Ikeda Y, Nakahata T. 1999. Differential effects of human granulocyte colony-stimulating factor (hG-CSF) and thrombopoietin on megakaryopoiesis and platelet function in hG-CSF receptor-transgenic mice. Blood 94:950–958.
Yu J, Vodyanik MA, Smuga-Otto K, Antosiewicz-Bourget J, Frane JL, Tian S, Nie J, Jonsdottir GA, Ruotti V, Stewart R, Slukvin II, Thomson JA. 2007. Induced pluripotent stem cell lines derived from human somatic cells. Science (New York, NY) 318:1917–1920.

Immunity
Resource

Functional Delineation and Differentiation Dynamics of Human CD4$^+$ T Cells Expressing the FoxP3 Transcription Factor

Makoto Miyara,[1,10] Yumiko Yoshioka,[1,9] Akihiko Kitoh,[1,9] Tomoko Shima,[1,9] Kajsa Wing,[1] Akira Niwa,[2] Christophe Parizot,[3] Cécile Taflin,[3] Toshio Heike,[2] Dominique Valeyre,[4] Alexis Mathian,[3] Tatsutoshi Nakahata,[2] Tomoyuki Yamaguchi,[1] Takashi Nomura,[1] Masahiro Ono,[1] Zahir Amoura,[5,6] Guy Gorochov,[3,6] and Shimon Sakaguchi[1,7,8,*]

[1]Department of Experimental Pathology, Institute for Frontier Medical Sciences
[2]Department of Pediatrics, Graduate School of Medicine
Kyoto University, Kyoto 606-8507, Japan
[3]Institut National de la Santé et de la Recherche Médicale (INSERM) UMR-S 945, Laboratoire AP-HP d'immunologie cellulaire et tissulaire, Hôpital Pitié-Salpêtrière, 75013 Paris, France
[4]Pneumology Department, AP-HP Hôpital Avicenne, 93000 Bobigny, France
[5]Internal Medicine Department, AP-HP Hôpital Pitié-Salpêtrière, 75013 Paris, France
[6]Pierre and Marie Curie University, UPMC Paris Universitas, 75005 Paris, France
[7]Core Research for Evolutional Science and Technology (CREST), Japan Science and Technology Agency, Kawaguchi 332-0012, Japan
[8]WPI Immunology Frontier Research Center, Osaka University, Suita 565-0871, Japan
[9]These authors contributed equally to this work
[10]Present address: Internal Medicine Department and Institut National de la Santé et de la Recherche Médicale (INSERM) UMR-S 945, Laboratoire AP-HP d'immunologie cellulaire et tissulaire, Hôpital Pitié-Salpêtrière, 75013 Paris, France
*Correspondence: shimon@frontier.kyoto-u.ac.jp
DOI 10.1016/j.immuni.2009.03.019

SUMMARY

FoxP3 is a key transcription factor for the development and function of natural CD4$^+$ regulatory T cells (Treg cells). Here we show that human FoxP3$^+$CD4$^+$ T cells were composed of three phenotypically and functionally distinct subpopulations: CD45RA$^+$FoxP3^{lo} resting Treg cells (rTreg cells) and CD45RA$^-$FoxP3^{hi} activated Treg cells (aTreg cells), both of which were suppressive in vitro, and cytokine-secreting CD45RA$^-$FoxP3^{lo} nonsuppressive T cells. The proportion of the three subpopulations differed between cord blood, aged individuals, and patients with immunological diseases. Terminally differentiated aTreg cells rapidly died whereas rTreg cells proliferated and converted into aTreg cells in vitro and in vivo. This was shown by the transfer of rTreg cells into NOD-scid-common γ-chain-deficient mice and by TCR sequence-based T cell clonotype tracing in peripheral blood in a normal individual. Taken together, the dissection of FoxP3$^+$ cells into subsets enables one to analyze Treg cell differentiation dynamics and interactions in normal and disease states, and to control immune responses through manipulating particular FoxP3$^+$ subpopulations.

INTRODUCTION

FoxP3-expressing CD4$^+$ thymus-derived naturally occurring regulatory T cells (Treg cells) play an indispensable role for the maintenance of self tolerance and immune homeostasis (Sakaguchi et al., 2008). They play crucial roles in human diseases, such as autoimmune disease, allergy, and cancer (Curiel et al., 2004; Ehrenstein et al., 2004; Kriegel et al., 2004; Miyara et al., 2005; Viglietta et al., 2004). Human natural Treg cells were initially defined according to their high expression of CD25 (Baecher-Allan et al., 2001; Dieckmann et al., 2001; Jonuleit et al., 2001; Levings et al., 2001; Ng et al., 2001; Taams et al., 2001), based on the finding that murine CD25$^+$CD4$^+$ T cells are highly suppressive (Sakaguchi et al., 1995). With the discovery of FoxP3 as a "master control gene" for CD4$^+$ Treg cell development and function (Fontenot et al., 2003; Hori et al., 2003; Khattri et al., 2003), detection of FoxP3 at the mRNA and protein level revealed that human CD25^{hi}CD4$^+$ T cells indeed express FoxP3 (Miyara et al., 2006; Roncador et al., 2005; Yagi et al., 2004). In contrast to murine FoxP3$^+$ Treg cells, however, human FoxP3$^+$ cells may not be functionally homogenous. For example, it has been reported that mere TCR stimulation can induce FoxP3 expression in apparently naive human FoxP3$^-$CD4$^+$ T cells without conferring suppressive activity (Allan et al., 2007; Gavin et al., 2006; Tran et al., 2007; Wang et al., 2007). Furthermore, some FoxP3$^+$ cells are phenotypically naive (e.g., CD45RA$^+$), present in cord blood as well as in peripheral blood of adults, and suppressive in vitro (Valmori et al., 2005), whereas other FoxP3$^+$ cells phenotypically resemble memory T cells (e.g., CD45RA$^-$) and are suggested to originate from peripheral memory FoxP3$^-$CD4$^+$ T cells (Vukmanovic-Stejic et al., 2006). To better understand the roles of FoxP3$^+$ T cells for the control of immune responses, it is necessary to determine whether FoxP3-expressing T cells in freshly isolated CD4$^+$ T cells are functionally heterogeneous, how functionally different subpopulations of FoxP3$^+$ cells can be reliably delineated, and how such

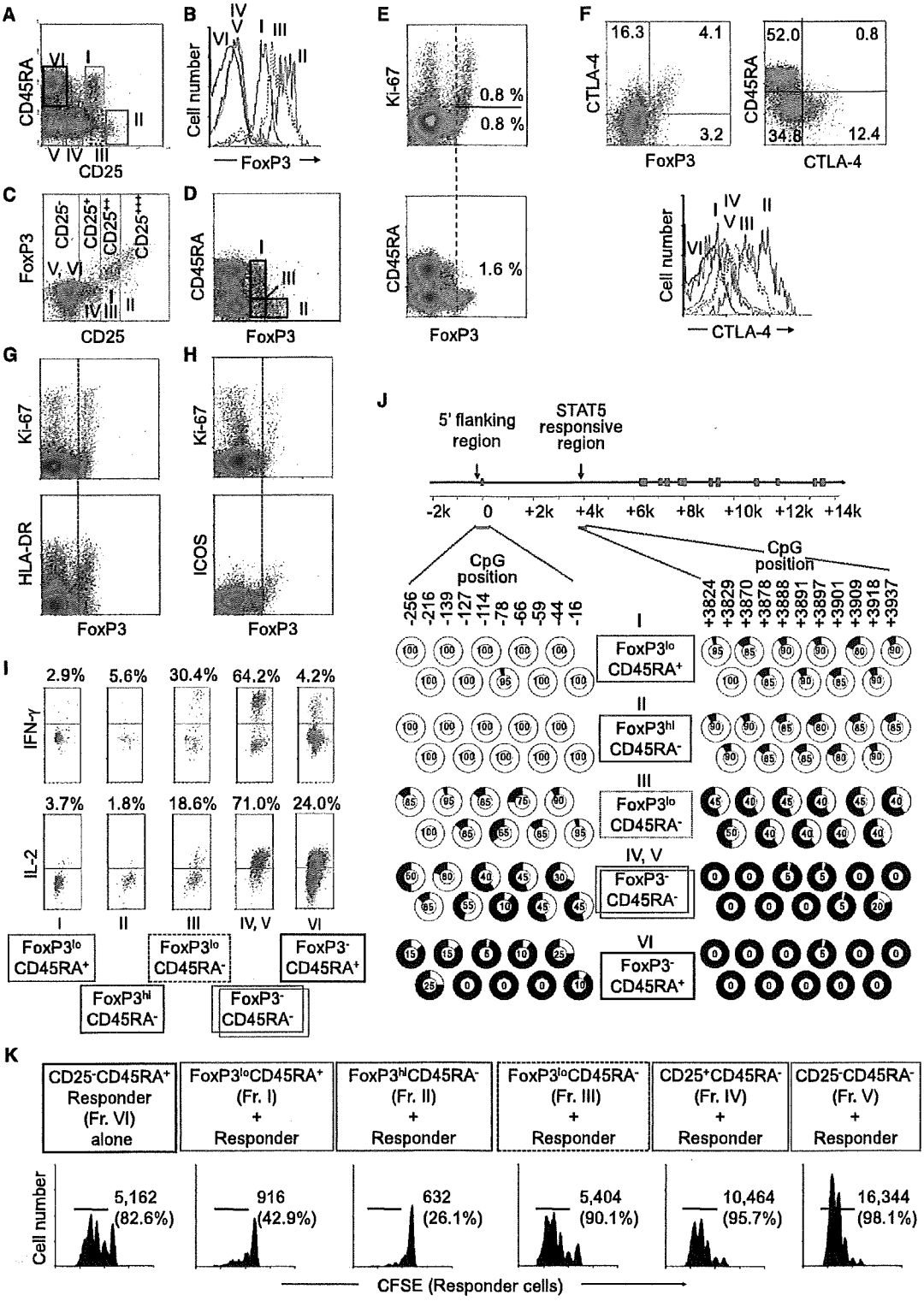
A
CD45RA
CD25
B
Cell number
FoxP3
C
FoxP3
CD25
D
CD45RA
FoxP3
E
Ki-67
0.8 %
0.8 %
CD45RA
1.6 %
FoxP3
F
CTLA-4
16.3
4.1
3.2
FoxP3
CD45RA
52.0
0.8
34.8
12.4
CTLA-4
Cell number
CTLA-4
G
Ki-67
HLA-DR
FoxP3
H
Ki-67
ICOS
FoxP3
I
IFN-γ
2.9%
5.6%
30.4%
64.2%
4.2%
IL-2
3.7%
1.8%
18.6%
71.0%
24.0%
I
II
III
IV, V
VI
FoxP3lo CD45RA+
FoxP3hi CD45RA-
FoxP3lo CD45RA-
FoxP3- CD45RA-
FoxP3- CD45RA+
J
5' flanking region
STAT5 responsive region
-2k
0
+2k
+4k
+6k
+8k
+10k
+12k
+14k
CpG position
-256 -216 -139 -127 -114 -78 -66 -59 -44 -16
+3824 +3829 +3870 +3878 +3888 +3891 +3897 +3901 +3909 +3918 +3937
I
FoxP3lo CD45RA+
II
FoxP3hi CD45RA-
III
FoxP3lo CD45RA-
IV, V
FoxP3- CD45RA-
VI
FoxP3- CD45RA+
K
CD25-CD45RA+ Responder (Fr. VI) alone
FoxP3loCD45RA+ (Fr. I) + Responder
FoxP3hiCD45RA- (Fr. II) + Responder
FoxP3loCD45RA- (Fr. III) + Responder
CD25+CD45RA- (Fr. IV) + Responder
CD25-CD45RA- (Fr. V) + Responder
Cell number
5,162 (82.6%)
916 (42.9%)
632 (26.1%)
5,404 (90.1%)
10,464 (95.7%)
16,344 (98.1%)
CFSE (Responder cells)

subsets differentiate and interact in physiological and disease states.

In this report, we show that human FoxP3$^+$CD4$^+$ T cells can be separated into three functionally and phenotypically different subpopulations based on the expression of FoxP3, cell surface phenotype, the degree of DNA methylation of the FoxP3 gene, DNA microarray profile, proliferation status in the physiological state, cytokine secreting capacity, TCR repertoire, and in vitro suppressive activity. These populations are (1) CD45RA$^+$FoxP3^{lo} resting Treg cells, (2) CD45RA$^-$FoxP3^{hi} activated Treg cells, and (3) cytokine-secreting CD45RA$^-$FoxP3^{lo} non-Treg cells. With this dissection of FoxP3$^+$ T cells into subpopulations, we show the dynamics of Treg cell differentiation in vitro, in vivo, and ex vivo in normal and disease states. The results indicate that functional and numerical analysis of each FoxP3$^+$ subset is essential for assessing immunological states, and that manipulation of a particular subset, rather than whole FoxP3$^+$ cells, helps to dampen or augment a variety of physiological and pathological immune responses.

RESULTS

Separation of FoxP3$^+$CD4$^+$ T Cells into Three Subpopulations by the Expression of FoxP3, CD25, and CD45RA

The combination of CD25 and CD45RA staining of CD4$^+$ T cells in peripheral blood lymphocytes (PBL) of normal healthy individuals revealed six subpopulations (Fraction [Fr.] I–VI) that expressed the FoxP3 protein at different amounts (Figures 1A and 1B). Among them, Fr. I, II, and III were FoxP3$^+$ (Figure 1B) and the degree of FoxP3 expression in these fractions were proportional to CD25 expression (Figure 1C). Notably, these three FoxP3$^+$ populations could be distinctly separated by the combination of FoxP3 and CD45RA staining; i.e., FoxP3^{lo}CD45RA$^+$ cells, which were CD25^{++} (Fr. I), FoxP3^{hi}CD45RA$^-$ cells, which were CD25^{+++} (Fr. II), and FoxP3^{lo}CD45RA$^-$ cells, which were CD25^{++} (Fr. III) (Figure 1D). The fractions could be prepared as live cells by cell sorting as CD25^{++}CD45RA$^+$, CD25^{+++}CD45RA$^-$, and CD25^{++}CD45RA$^-$ cells, respectively (Figure S1A available online). Purified Fr. I, II, and III populations expressed FoxP3 transcripts to a similar degree irrespective of different amounts of FoxP3 protein expressed in each population (Figure 1B; Figure S1B). Fr. IV formed a distinct population as CD25$^+$FoxP3$^-$ cells (Figure 1C), but it was not well demarcated from Fr. V by CD45RA or CD25 staining (Figure 1A). Therefore, we analyzed Fr. IV and V together in the functional examination of FoxP3$^+$ subsets (see below).

Assessment of the proliferative status of each subpopulation in the physiological state by detecting the expression of Ki-67, a nuclear protein expressed in cells ready to proliferate and at a higher amount in actually proliferating cells (Figure S2), revealed that about half of the cells in Fr. II were proliferating whereas the cells in Fr. I and III were not (red dotted line in Figure 1E). Fr. II expressed intracellular CTLA-4 to the highest degree whereas Fr. I hardly expressed the molecule (Figure 1F). Furthermore, Fr. II corresponded to HLA-DR-expressing and also ICOS-expressing FoxP3$^+$ cells as reported by others (Figures 1G and 1H; Baecher-Allan et al., 2006; Ito et al., 2008).

Analysis of cytokine production by each fraction showed that Fr. II scarcely produced IL-2 or IFN-γ. Among FoxP3^{lo} cells, Fr. I was poor producer of IL-2 and IFN-γ whereas Fr. III produced high amounts of these cytokines (Figure 1I; Figure S3).

The 5′ flanking region and a STAT5-responsive region in the intron 1 of the *FOXP3* gene are critical for induction and enhancement of FoxP3 expression by TCR and IL-2 stimulation (Floess et al., 2007; Mantel et al., 2006; Zorn et al., 2006). Analysis of the DNA methylation status of these regions in each fraction prepared from a male donor showed that the CpG methylation sites in the regions were completely demethylated in Fr. I and Fr. II (Figure 1J). The 5′ flanking region of Fr. III was also highly demethylated, although the demethylation pattern was less uniform compared with Fr. I and II. In contrast, their STAT5-responsive region was less demethylated than other FoxP3$^+$ subsets. In addition, memory-like CD25$^+$ and CD25$^-$ CD45RA$^-$CD4$^+$ non-Treg cells (Fr. IV, V), which were FoxP3$^-$, had their 5′ flanking region moderately demethylated whereas the STAT5 responsive region was virtually completely methylated. Both regions were highly methylated in naive Fr. VI. These findings were confirmed by analysis of individual clones isolated from each subpopulation (Figure S4). The results collectively

Figure 1. Delineation of FoxP3$^+$CD4$^+$ T Cells into Subsets by Cell Surface Molecules, Proliferative State, Cytokine Production, Methylation Status of the *FOXP3* Gene, and In Vitro Suppressive Activity

(A–D) Six subsets of CD4$^+$ T cells defined by the expression of CD45RA and CD25: pink line (Fraction [Fr.] I), CD25^{++}CD45RA$^+$ cells; bold red line (Fr. II), CD25^{+++}CD45RA$^-$ cells; broken brown line (Fr. III), CD25^{++}CD45RA$^-$ cells; green line (Fr. IV), CD25$^+$CD45RA$^-$ cells; blue line (Fr. V), CD25$^-$CD45RA$^-$ cells; black line (Fr. VI), CD25$^-$CD45RA$^+$ cells. Expression of FoxP3 (B), CD25 and intracellular FoxP3 (C), and CD45RA and FoxP3 (D) in each fraction shown in (A). Data are representative of 19 blood donors.

(E) Flow cytometry of the expression of nuclear Ki-67 and FoxP3 in CD4$^+$ T cells. Red broken line separates Ki-67$^+$FoxP3^{hi} from Ki-67$^-$FoxP3^{lo} cells and CD45RA$^+$FoxP3^{lo} from CD45RA$^-$FoxP3^{hi} cells. The percentages of Ki-67$^+$ and Ki-67$^-$FoxP3^{hi} cells among CD4$^+$ cells are indicated in the top panel and the percentage of FoxP3^{hi}CD45RA$^-$ cells in the bottom panel.

(F) Flow cytometry of the expression of intracellular CTLA-4 and FoxP3 (top left); CD45RA and CTLA-4 (top right) by CD4$^+$ T cells; and expression of CTLA-4 by each fraction defined in (A)–(D) (bottom). Numbers indicate percent of cells in each quadrant.

(G and H) Expression of Ki-67 and FoxP3 (top) and of HLA-DR or ICOS and FoxP3 (bottom). Red broken line separates Ki-67$^+$FoxP3^{hi} from Ki-67$^-$FoxP3^{lo} cells and HLA-DR$^-$FoxP3^{lo} from HLA-DR$^+$FoxP3^{hi} cells (G) or ICOS$^-$FoxP3^{lo} from ICOS$^+$FoxP3^{hi} cells (H).

(I) Production of IFN-γ, IL-2 by each fraction after stimulation with PMA + Ionomycin, and percent of cytokine-secreting cells in each fraction is shown. Data are representative of six independent experiments.

(J) Analysis of DNA methylation status at 5′ flanking region (left) and STAT5-responsive (right) region of the *FOXP3* gene in FoxP3-expressing or -nonexpressing CD4$^+$ T cell subsets (Figure S1) from PBMCs of one healthy male donor. Percentages of clones displaying demethylation of indicated CpG methylation sites are indicated and depicted in white in sector graphs. 19 to 20 clones were sequenced from each CD4$^+$ T cell subset.

(K) CFSE dilution by 10^4 labeled CD25$^-$CD45RA$^+$CD4$^+$ responder T cells assessed after 84–90 hr of TCR-stimulated coculture with indicated CD4$^+$ T cell subset at a 1 to 1 ratio. Cell number and percentage of dividing cells per well are indicated. Data are representative of 12 separate experiments.

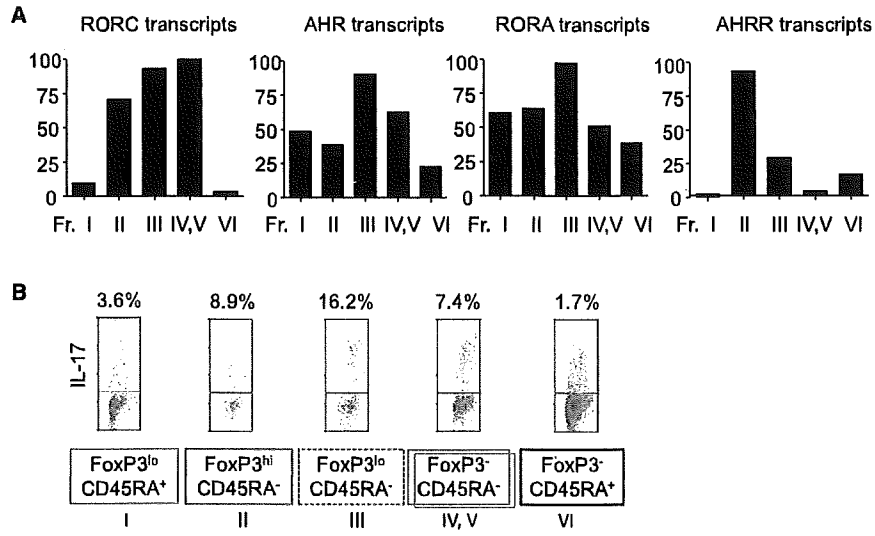

Figure 2. CD45RA$^-$FoxP3^{lo}CD4$^+$ T Cells Contain Cells with Th17 Cell Potential

(A) The amounts of transcripts of indicated genes in separated CD4$^+$ T cell subsets were assessed by quantitative PCR.

(B) Flow cytometry of the production of IL-17 by gated CD4$^+$ T cell subsets after stimulation with PMA + ionomycin for 5 hr. Percentages of cytokine-secreting cells are shown. Data are representative of six independent experiments.

indicate that Fr. I and II are active in FoxP3 gene transcription and close in their differentiation stage, and that, compared with these fractions, Fr. III may be less capable of maintaining FoxP3 expression in the presence of IL-2 and STAT5 signaling.

To assess the in vitro suppressive potency of each fraction, we measured the extent of CFSE dilution of labeled naive CD25$^-$CD45RA$^+$CD4$^+$ T cells (hereafter called responder cells) cocultured with an equal number of each fraction and stimulated for 4 days (Figure 1K). Fr. I and II (isolated as CD25^{++}CD45RA$^+$ and CD25^{+++}CD45RA$^-$ cells, respectively, as shown in Figure S1) potently suppressed the proliferation of responder cells, whereas Fr. III, IV, and V did not and even enhanced the responder proliferation. The inability of Fr. III (CD45RA$^-$Foxp3^{lo} cells) to suppress was confirmed by using CD127 as an additional marker for purifying FoxP3-expressing cells from CD4$^+$ T cells (Figure S5; Liu et al., 2006; Seddiki et al., 2006).

Taken together, three distinct subpopulations of FoxP3$^+$CD4$^+$ T cells can be defined in human PBL by the expression of CD45RA and FoxP3 as summarized in Table S1; i.e., Fr. I: CTLA-4^{lo}Ki-67$^-$CD45RA$^+$FoxP3^{lo} T cells; Fr. II: CTLA-4^{hi}CD45RA$^-$FoxP3^{hi} cells, both of which possess a fully functional *FOXP3* gene, hardly secrete cytokines, and potently suppress proliferation; and Fr. III: CTLA-4^{int}CD45RA$^-$FoxP3^{lo} T cells, which secrete cytokines, are much less active in the expression of the *FOXP3* gene under the control via STAT5, and do not suppress proliferation in vitro. Based on their phenotypic and functional characteristics, Fr. I and Fr. II can be designated as resting Treg cells (rTreg cells) and activated Treg cells (aTreg cells), respectively.

FoxP3^{lo}CD45RA$^-$ Nonregulatory T Cells Contain Cells with Th17 Cell Potential

DNA microarray analysis of each fraction showed that the gene expression patterns in the three FoxP3-expressing subpopulations were distinct (Figure S6A). Quantitative assessment of mRNA expression of differentially expressed genes revealed that the expression of RORC, a key transcription factor in Th17 cell lineage (Ivanov et al., 2006), was highly upregulated in Fr. II and III, indicating that RORC-FoxP3 double-positive population, which was recently described in mice (Yang et al., 2008a; Zhou et al., 2008), exists in humans as well in Fr. II and III (Figure S6B). Transcripts encoding RORα and AHR, both of which contribute to Th17 cell differentiation in mice (Veldhoen et al., 2008; Yang et al., 2008b), were highly upregulated in Fr.III, further indicating that this population contains cells with Th17 cell potential (Figure 2A). Also of note is that Fr. II specifically expressed high amounts of AHR repressor transcripts, suggesting that Treg cell differentiation might accompany an inhibition of Th17 cell differentiation via expression of AHR repressor. Assessment of cytokine production revealed that Fr. III was the highest producer of IL-17 even compared with naive FoxP3$^-$CD45RA$^+$ (Fr. VI) or memory-like FoxP3$^-$CD45RA$^-$CD4$^+$ non-Treg cells (Fr. IV and V) (Figure 2B; Figure S3).

Thus, DNA microarray profiling of FoxP3$^+$ subpopulations supports the relevance of separating FoxP3$^+$CD4$^+$ T cells into three subsets. Further, regarding the cell lineage relationship of FoxP3$^+$ cells and Th17 cells, Fr. III contains FoxP3-RORγ double-positive cells with a Th17 cell potential, in addition to IL-2- and/or IFN-γ-producing cells (Figure 1I).

Resting Treg Cells Proliferate whereas Activated Treg Cells Die while Suppressing In Vitro

As shown in Figure 1E, fresh Fr. I cells (rTreg cells) did not express Ki-67. However, when they were cocultured with responder cells and TCR stimulated, all the FoxP3-expressing cells became Ki-67$^+$ on day 4, indicating that rTreg cells proliferate (Figure S7). Assessment of proliferation by CFSE dilution during 4 days of culture also revealed that both aTreg cells

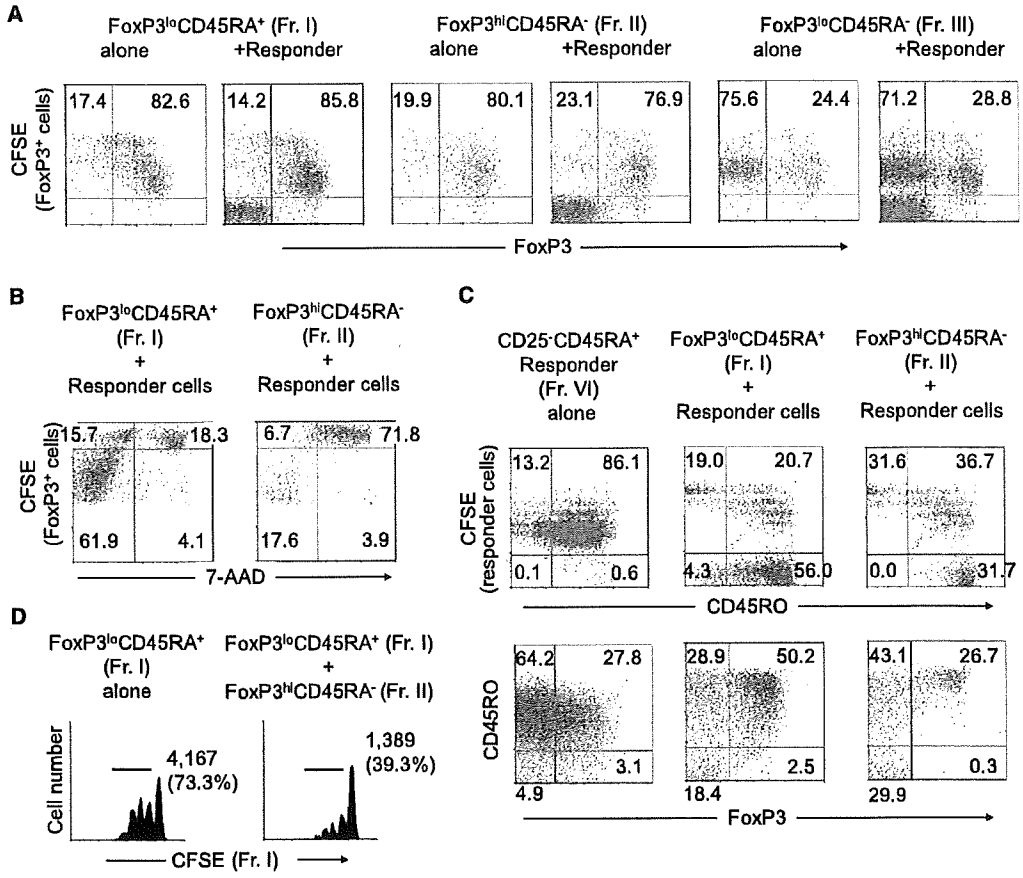

Figure 3. In Vitro Properties of FoxP3+ Subpopulations

(A) CFSE dilution by rTreg or aTreg cells and intracellular expression of FoxP3 were analyzed after 4 days TCR stimulation in the absence or presence of nonlabeled responder cells. Percentages of FoxP3- and of FoxP3+ cells among CFSE-labeled cells are indicated.

(B) Viability assessed by 7-AAD staining of CFSE-labeled CD45RA+FoxP3lo (left) or CD45RA-FoxP3hi Treg cells (right) cocultured with nonlabeled responder cells for 4 days. Only CFSE-labeled cells are shown. Numbers indicate percentage in each quadrant. Data shown are representative of five independent experiments.

(C) CFSE dilution, surface CD45RO, and intracellular FoxP3 expression by CFSE-labeled responder cells cultured alone or cocultured with unlabeled Treg cell subsets for 4 days. Numbers indicate percentage in each quadrant.

(D) CFSE dilution of labeled rTreg cells cultured alone or with aTreg cells at a 1 to 1 ratio. Numbers and percentage of proliferating cells are indicated. Data shown in (B) and (D) are representative of five independent experiments.

(Fr. II) and rTreg cells (Fr. I) gave rise to CFSE-diluting FoxP3+ cells when cultured alone (Figure 3A). In addition, rTreg cells showed more active proliferation than did aTreg cells in the presence of responder cells. In contrast with rTreg or aTreg cells, most (~70%) of CD45RA-FoxP3loCD4+ T cells (Fr. III) did not express FoxP3 during their proliferation, indicating that FoxP3 expression in the majority of Fr. III cells may not be stable in concordance with the methylation status of their *FOXP3* gene (Figure 3A).

Based on the finding that very few aTreg cells (Fr. II) were detectable after 4 days of culture (Figure S7), we assessed the viability of Treg cells by measuring incorporation of 7-AAD by CFSE-labeled rTreg or aTreg cells cultured with responder cells (Figure 3B). The majority (~75%) of aTreg cells were positive for 7-AAD. By contrast, although a fraction (~20%) of rTreg cells were nonproliferative and 7-AAD+, the majority of proliferating rTreg cells (~60%) were 7-AAD- (Figure 3B). In addition to proliferation, rTreg cells showed increased expression of FoxP3 (Figure 3A), CD45RO (Figure 3C), and intracellular CTLA-4 (Figure S8). High expression of CD45RO was secondary to activation because rTreg cells, which were CD45RA+, did not express CD45RO when freshly isolated from peripheral blood (Figure S9). Further, when CFSE-labeled rTreg cells (Fr. I) were cultured with nonlabeled aTreg cells (Fr. II), the latter substantially suppressed the proliferation of the former (Figure 3D).

Taken together, rTreg cells are not anergic and are able to proliferate upon TCR stimulation. They acquire a Ki-67+FoxP3hi aTreg cell phenotype and exert suppression during and after their proliferation and conversion to aTreg cells, which die after proliferation and exertion of suppression. Activated Treg cells also suppress the proliferation of resting Treg cells in a negative feedback fashion. Thus, in addition to different cell surface phenotypes, rTreg and aTreg cells possess different cell fates despite their comparable in vitro suppressive activity when assessed separately.

In Vivo Conversion of rTreg Cells to aTreg Cells and Differentiation of a Small Fraction of FoxP3$^-$ Cells to FoxP3$^+$ Cells

Next, to investigate whether the in vitro conversion of rTreg cells to aTreg cells could also occur in vivo, we transferred human PBMCs containing CFSE-labeled CD4$^+$ T cells into NOG (Nod-scid-common γ-chain-deficient) mice and analyzed their splenocytes 5 days after transfer (Hiramatsu et al., 2003). FoxP3^{hi}CD4$^+$ T cells recovered in the recipients were largely CD25^{hi} and CD45RO$^+$ (data not shown) and mostly confined to Ki-67$^+$CFSE-diluting cells, which had divided more than 6 times after transfer (Figure 4A). In addition, most CD4$^+$ T cells expressing low amounts of FoxP3 had not proliferated. These findings correspond to the in vitro findings that FoxP3^{hi} aTreg cells found in PBMCs were highly proliferative and that FoxP3^{lo}CD4$^+$ T cells were Ki-67$^-$ in PBMCs (Figure 1E), suggesting that, upon activation, rTreg cells upregulate FoxP3 expression and then proliferate. We also examined the behavior of Treg cells or whole FoxP3$^+$ cells when injected without other effector CD4$^+$ T cells. Neither population proliferated, indicating that the maintenance and proliferation of FoxP3-expressing cells requires the presence of other CD4$^+$ T cells in vivo (Figure S10).

Similar analysis of PBMCs containing CFSE-labeled rTreg cells, prepared as shown in Figure 1A and Figure S1, showed that they proliferated in vivo and upregulated the expression of FoxP3 and CD45RO along several cell divisions (Figure 4B and data not shown). Because most FoxP3^{hi} cells were detected in CFSE-negative cells after transfer of CFSE-labeled CD4$^+$ T cells or rTreg cells (Figures 4A and 4B), we attempted to determine whether rTreg cells were the major source of CFSE-negative FoxP3^{hi} cells. Injection of PBMCs containing CFSE-labeled CD4$^+$ T cells devoid of rTreg cells revealed a much lower number of FoxP3^{hi} cells when compared with injection of whole CD4$^+$ T cells, indicating that most FoxP3^{hi} aTreg cells derive from rTreg cells (Figure 4C).

Further, to investigate whether the conversion of FoxP3$^-$ to FoxP3$^+$ in CD4$^+$ T cells could occur in vivo, we transferred PBMCs containing CFSE-labeled FoxP3$^-$ CD127^{hi}CD4$^+$ T cells together with nonlabeled FoxP3$^+$ cells (as CD25^{hi}CD127^{lo} cells) in NOG mice and examined whether FoxP3$^-$CD4$^+$ T cells could upregulate FoxP3 in vivo (Figure 4D). Although most CFSE-labeled cells remained FoxP3$^-$, a small number of cells upregulated FoxP3 from low to high amounts. Injection of only CFSE-labeled CD4$^+$FoxP3$^-$ cells confirmed that a small fraction (<1%) of CD4$^+$FoxP3$^-$ cells indeed divided at least 6 times to give rise to FoxP3^{hi} cells (Figure 4E). Taken together, these results indicate that rTreg cells convert to aTreg cells and that only a small fraction of aTreg cells derives from FoxP3$^-$CD4$^+$ non-Treg cells in vivo.

In Vivo Conversion of rTreg Cells to aTreg Cells in a Normal Human Individual

To obtain further evidence for the in vivo rTreg to aTreg cell conversion in normal humans, we attempted to trace clonotypes of each Treg cell fraction in a single individual at separate time points. Cells in rTreg cells (Fr. I), aTreg cells (Fr. II), and also FoxP3$^-$ non-Treg CD4$^+$ T cells (Fr. IV, V, VI) that expressed the same TCRBV5 family were sorted from a single healthy individual at 18 month intervals. Single-cell RT-PCR and DNA sequencing of the amplicons was performed to compare TCRBV5 CDR3 regions in each sorted subset. Given the small size of the sample, the analysis was able to monitor dominant clones only. First, we observed that rTreg (Fr. I) and aTreg (Fr. II) cell subsets shared few dominant clonotypes at a given time point. Second, we found that a clonotype initially detected in the rTreg cell subset was found dominant 18 months later in the aTreg but not in the rTreg cell subset. The TCR repertoire being potentially so heterogeneous and the sample size being so limited (45 to 137 cells analyzed in each subset), it is highly improbable that T cell clones with identical TCR sequences could be found in the same subsets only by chance. Indeed, when random samples of conventional CD4$^+$ T cells were similarly compared, shared clonotypes were never found in this individual (Figure 5; Table S2). The analysis also revealed that none of the clonotypes found in FoxP3$^-$ cells was found in aTreg cells 18 months later, indicating that if conversion of FoxP3$^-$CD4$^+$ T cells ever occurs in vivo, it may not be a frequent phenomenon compared with the conversion of rTreg cells to aTreg cells (Figure 5).

Based on these observations in Figures 4 and 5, we conclude that most FoxP3^{hi} aTreg cells are derived from recently activated and vigorously proliferating rTreg cells, and that only a minority of aTreg cells can develop from FoxP3$^-$CD4$^+$ non-Treg cells in vivo. The result also indicates that the TCR repertoire of Treg cells, in particular that of aTreg cells, adaptively changes in normal individuals.

Variations in Human rTreg and aTreg Cell Populations under Normal and Disease Conditions

We then attempted to determine whether the dissection of FoxP3$^+$ T cells in adult humans into Fr. I–III based on CD45RA and FoxP3 expression was pertinent to the analysis of the dynamics of Treg cell generation and differentiation in ontogeny, aging, and disease states.

Although rTreg cells were highly prevalent in cord blood, we could easily detect Ki-67$^+$FoxP3^{hi}CD45RA$^-$CD4$^+$ T cells that corresponded to aTreg cells in adults. We failed to confirm the previously reported finding that all CD25$^+$CD4$^+$ T cells were FoxP3$^+$ in cord blood (Fritzsching et al., 2006). However, CD4$^+$ T cells expressing the highest amounts of CD25 contained only FoxP3$^+$ cells and CD127 expression efficiently separated FoxP3$^+$CD25$^+$ from FoxP3$^-$CD25$^+$CD4$^+$ T cells (Figure 6A). IFN-γ production was barely detectable in whole CD4$^+$ T cells whereas IL-2 production was observed in FoxP3^{lo}CD45RA$^-$CD4$^+$ T cells as in adults (data not shown).

Analysis of the expression of CD31 (PECAM-1), which is known to be expressed in recent thymic emigrants but lost during their post-thymic peripheral expansion (Kimmig et al., 2002), revealed that almost all CD31$^+$FoxP3$^+$CD4$^+$ T cells in adult PBL were confined in the CD45RA$^+$FoxP3^{lo} population (Fr. I). This finding suggests that the majority of rTreg cells may be recently derived from the thymus (Figure 6B).

The proportion of rTreg cells (Fr. I) among CD4$^+$ T cells was decreased in aged donors (1.1% ± 0.59%, n = 12 versus 2.40% ± 0.89% in healthy donors, n = 29; $p < 0.0001$) whereas that of aTreg cells (Fr. II) was increased (2.48% ± 1.07% versus 1.63% ± 0.53%; $p = 0.01$; Figures 6C and 6D).

We next applied our new definition of FoxP3$^+$ T cell subsets to the analysis of two pathological conditions that reportedly show

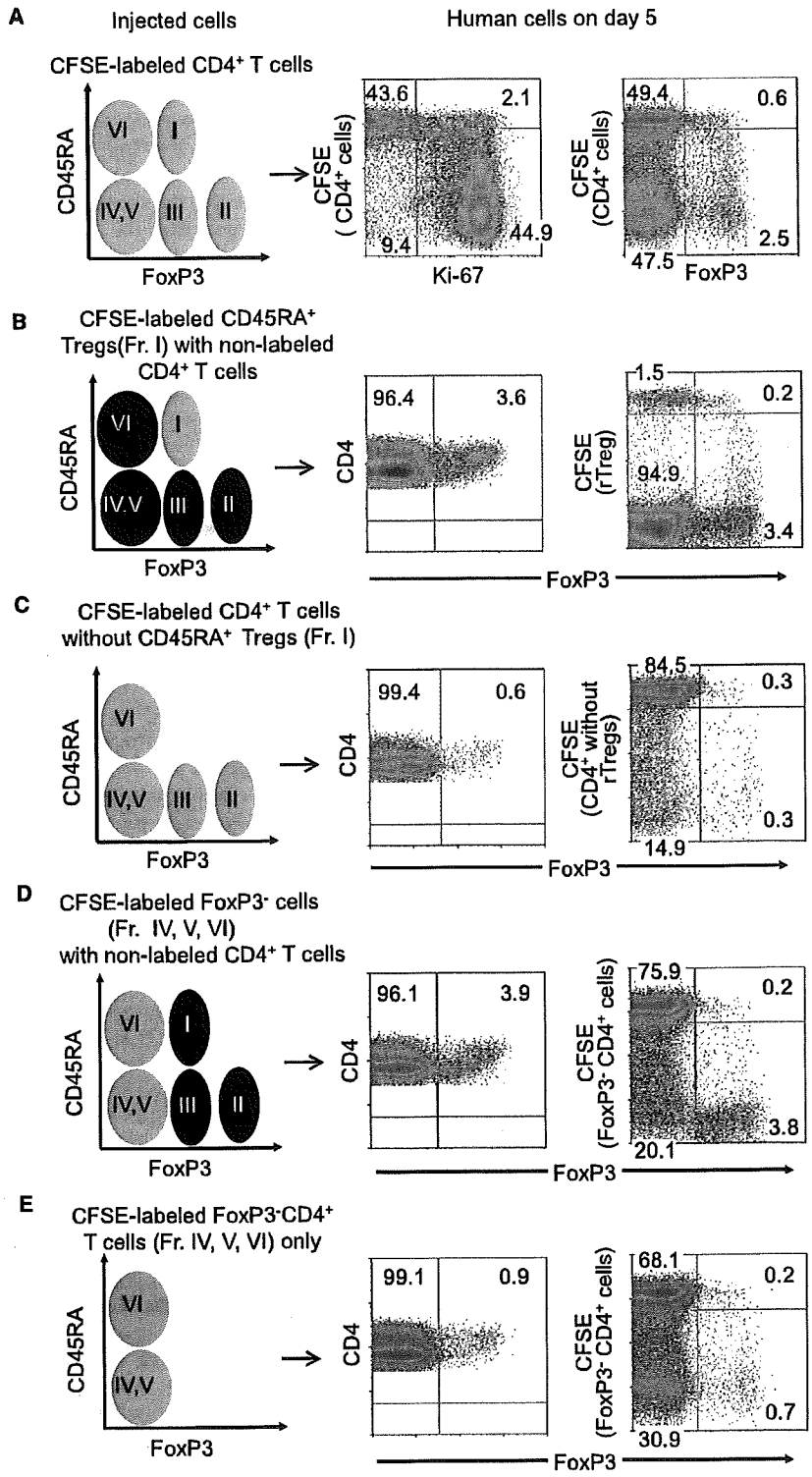

Figure 4. In Vivo Conversion of Treg Cell Phenotype in NOG Mice

PBMCs containing human CD4+ T cells were i.v. injected in NOG mice and collected in the spleen 5 days later. In schematic representations (left) of flow cytometric profiles of injected cells before transfer, CFSE-labeled CD4+ T subsets are depicted in green and injected with nonlabeled cells in black. Flow cytometry of human CD4+ T cells in the spleen after transfer of PBMCs containing CFSE-labeled human whole CD4+ T cells (A) or indicated CFSE-labeled CD4+ T cell subpopulations (B–E) into NOG mice. Numbers indicate percentage in each quadrant (right). Representative data of four mice transferred with PBMCs containing CFSE-labeled CD4+ T cells isolated from three different donors (A), and mice (two for each condition) transferred with PBMCs with indicated CFSE-labeled T cell populations obtained from two different donors (B–E).

different patterns of Treg cell involvement (Miyara et al., 2005, 2006). In sarcoidosis, a granulomatous disease of unknown origin, patients with active disease showed a considerable increase in the proportion of aTreg cells among CD4+ T cells (4.67% ± 3.35%, n = 41; $p < 0.0001$) combined with a high prevalence of Ki-67+FoxP3^{hi}CD4+ T cells and a decrease in the proportions of rTreg cells (1.48% ± 0.89%; $p < 0.0001$). In active systemic lupus erythematosus (SLE), a prototype of systemic autoimmune disease, there was a decrease in the proportion of aTreg cells (1.24 ± 0.72; n = 15; $p = 0.006$) and an increase in the proportions of rTreg cells (4.2 ± 1.86; $p = 0.0008$). Notably, CD45RA$^-$FoxP3^{lo} non-Treg cell fraction (Fr. III) increased to form a distinct population in active SLE (10.37% ± 9.3% versus 3.04 ± 1.1 in healthy donors; $p < 0.0001$; Figures 6C and 6D).

Thus, distinction of Treg cell subsets simply based on the combination of CD45RA and FoxP3 expression is highly informative in assessing the dynamics of Treg cell differentiation under physiological and disease conditions.

DISCUSSION

We have shown in this report that FoxP3+ cells in human PBL are heterogeneous in function and include not only suppressive T cells but also nonsuppressive ones that abundantly secrete proinflammatory cytokines such as IL-17. Further, Treg cells functionally and phenotypically differentiate within the FoxP3+ population. This functional heterogeneity and differentiation dynamics can be clearly shown by separating FoxP3+ cells into three subsets based on the expression of FoxP3 and CD45RA (or CD45RO), which

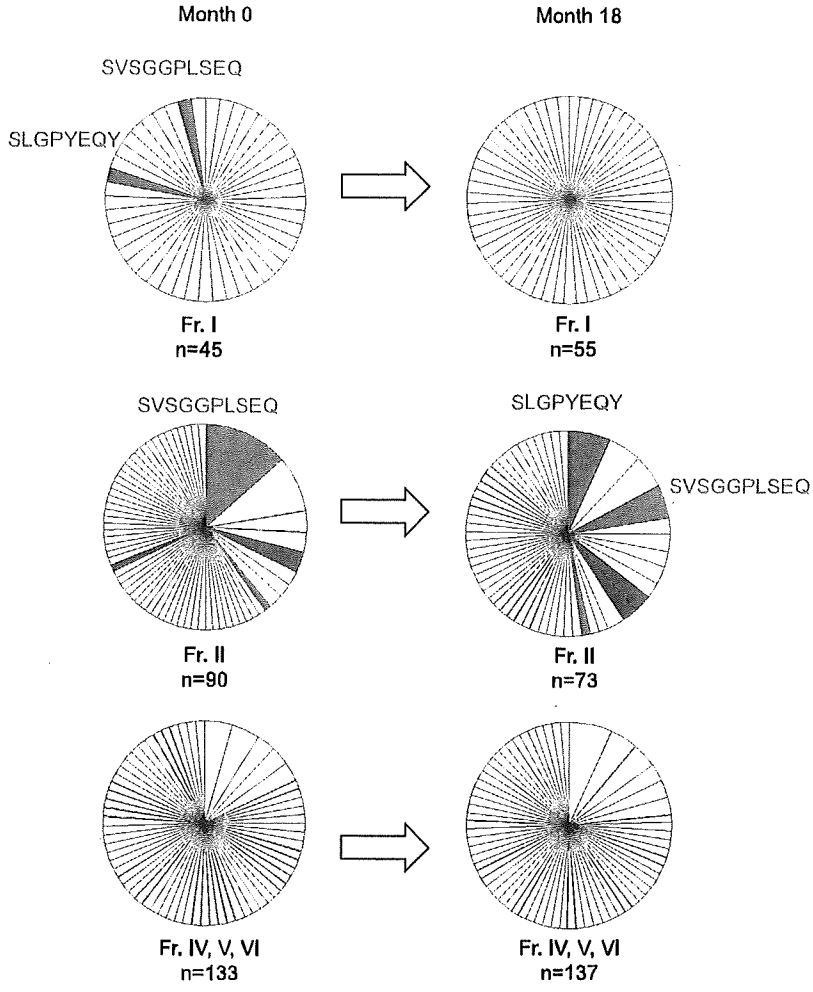

Figure 5. Longitudinal TCR Repertoire Analysis in FoxP3+ Cell Subpopulations

TCRBV5+CD4+ T cells belonging to indicated Treg or non-Treg cell fractions were FACS sorted as a single cell at indicated time points into wells of PCR plates. By RT-PCR and TCR sequencing, the frequencies of individual sequences were assessed. Empty slices correspond to sequences that were found only once in only one subset. Persistent clones are color highlighted. Slice size is proportional to the number of occurrences of the corresponding TCR sequences. The total number of sequences successfully analyzed in each subset is indicated.

controls signaling thresholds in lymphocytes, hence their state of differentiation and activation (Hermiston et al., 2003). The three subpopulations are CD45RA$^-$FoxP3^{hi}CD4$^+$ activated Treg cells and CD45RA$^+$FoxP3^{lo}CD4$^+$ resting Treg cells, both of which are potently suppressive in vitro, and cytokine-secreting nonsuppressive CD45RA$^-$FoxP3^{lo}CD4$^+$ non-Treg cells.

The distinction of FoxP3$^+$ subpopulations revealed the differentiation pathways of Treg cell subpopulations. First, most of FoxP3^{hi} aTreg cells originate from rTreg cells as shown in vitro and in vivo, although some FoxP3^{hi} Treg cells may arise from FoxP3$^-$CD4$^+$ non-Treg cells (Vukmanovic-Stejic et al., 2006). Second, a large proportion of FoxP3^{hi} aTreg cells is highly proliferative in vivo and appears to be recently activated, although most rTreg cells are in a resting state. Once rTreg cells are stimulated, they upregulate FoxP3 expression, differentiate to aTreg cells, and proliferate. In addition to these results obtained by direct ex vivo analysis of the subpopulations and by their transfer to NOG mice, our longitudinal study of the repertoire of a particular TCR Vβ subfamily in a single individual provides further evidence that the conversion of rTreg to aTreg cells physiologically occurs in vivo. In our current analysis, dominant clones found in the rTreg cell population were found 18 months later in the aTreg, but not rTreg, cell population. This indicates that the clones have preferentially expanded after differentiating to aTreg cells, as suggested by the high rate of Ki-67$^+$ cells in the aTreg cell population. The presence of such dominant T cell clones over a long period of time is a key feature of the aTreg cell population (C.P. and G.G., unpublished data). This also indicates that the TCR repertoire of Treg cells adaptively changes with clonal expansion especially in aTreg cells. Considering that aTreg cells rapidly die in vitro and that the immune system is constantly challenged by exogenous and endogenous antigens, it is highly likely that the maintenance of the pool of aTreg cells is the consequence of a tight balance between the constant development of aTreg cells from activated and proliferating rTreg cells and their death after exerting suppression. Further, aTreg cells control rTreg cell expansion in a feedback manner, contributing to the maintenance of the balance. FoxP3^{hi} aTreg cells thus appear to be terminally differentiated Treg cells; yet it remains to be determined whether the aTreg cell population contains a memory type long-living Treg cells. Given that aTreg cells die rapidly and that rTreg cells are highly proliferative upon stimulation, attempts to expand Treg cells ex vivo for cell therapy should be focused on rTreg cells as proposed by others (Hoffmann et al., 2006). It needs to be determined whether rTreg cells are constantly produced by the thymus, or whether they have a high renewal capacity in the periphery, or both.

Our study has clearly shown that human FoxP3$^+$CD4$^+$ T cells contain cytokine-secreting nonsuppressive effector T cells that display low expression of FoxP3. These nonsuppressive FoxP3^{lo}CD45RA$^-$CD4$^+$ T cells (Fr. III) may correspond to recently described activation-induced FoxP3-expressing cells that transiently express FoxP3 in vitro (Allan et al., 2007; Gavin et al., 2006; Tran et al., 2007; Wang et al., 2007). Supporting this notion, although the 5′ flanking region of the *FOXP3* gene in FoxP3^{lo}CD45RA$^-$CD4$^+$ T cells is highly demethylated, the STAT5-responsive region is poorly demethylated, suggesting that they may be unstable in maintaining FoxP3 expression through

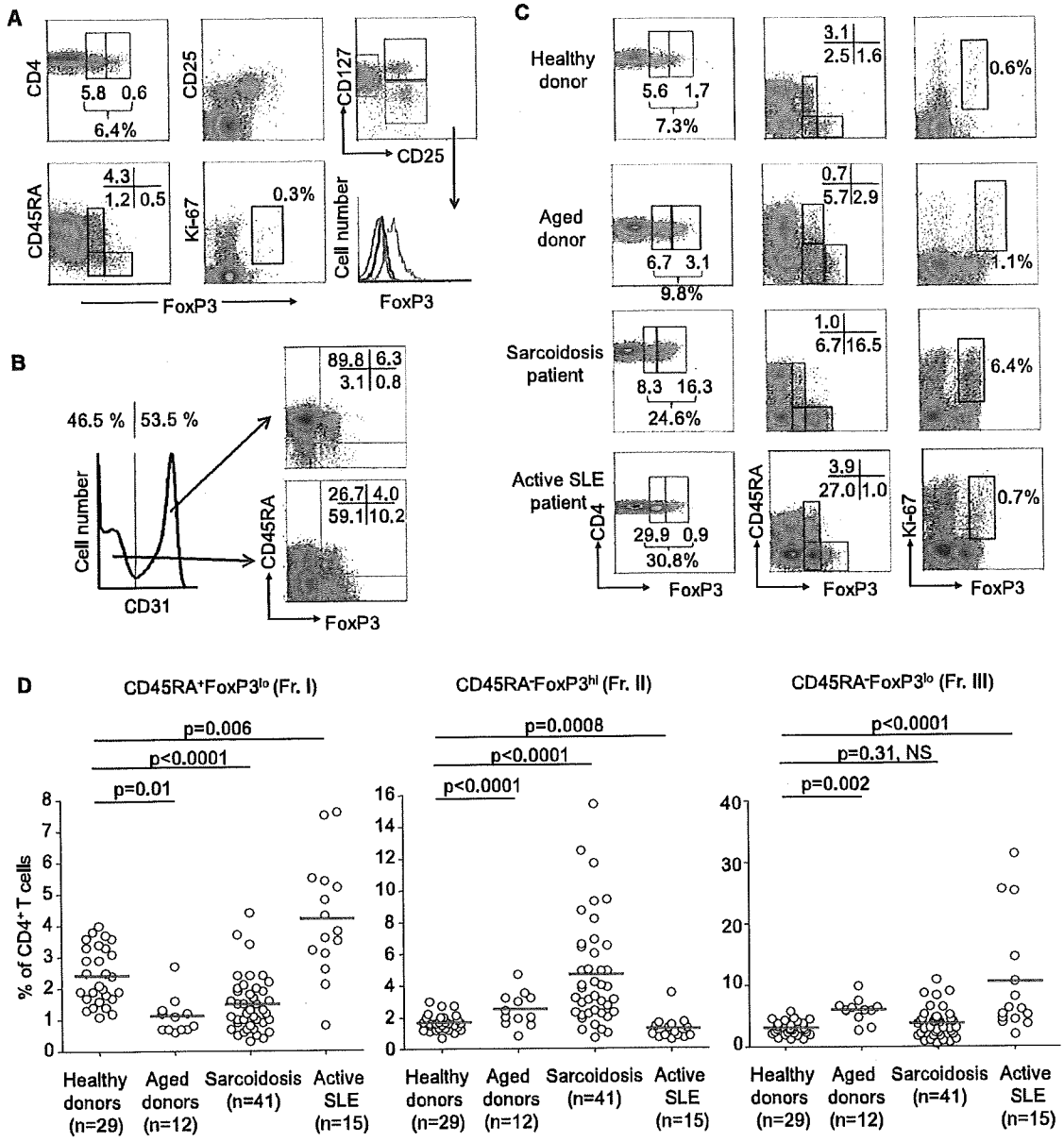

Figure 6. Variations in FoxP3+ Cell Subpopulations under Physiological and Disease Conditions

(A) Flow cytometry of PBMCs gated on CD4+ T cells isolated from cord blood. A representative of four samples.

(B) Expression of CD45RA and FoxP3 by gated CD31+ or CD31− CD4+ T cells. Numbers indicate percentage in each quadrant. A representative of four independent experiments.

(C) Flow cytometry of PBMCs gated on CD4+ T cells isolated from a 29-year-old healthy adult, an 88-year-old donor, and two patients with active sarcoidosis or active SLE. Percentage of each quadrant in each staining combination is shown.

(D) Percentages of each FoxP3+ subset among CD4+ T cells in indicated numbers of patients with active sarcoidosis, active SLE, aged donors (between 79 and 90 years old), and healthy donors (between 18 and 40 years old). Red horizontal bars represent mean percentage. Statistical comparisons were performed by nonparametric Mann-Whitney U test. NS, not significant.

STAT5 signaling. The notion is also supported by recent reports showing that activation-induced FoxP3+CD4+ T cells have *FOXP3* DNA significantly less demethylated than bona fide Treg cells (Baron et al., 2007; Janson et al., 2008). In addition, although CD127 is a convenient marker for isolating FoxP3+ cells as CD25hiCD127loCD4+ T cells (Liu et al., 2006; Seddiki et al., 2006), it is of note that they also include FoxP3+ non-Treg cells. We therefore propose that the combination of CD25 and CD45RA is so far the best markers for purifying human FoxP3+ Treg cells as rTreg and aTreg cells.

We noticed in microarray analysis that RORC, the human ortholog of murine RORγt, a major transcription factor for Th17 cell differentiation (Ivanov et al., 2006), was highly upregulated in both Fr. II and III and much less in Fr. I. Indeed, FoxP3^{lo} memory-like non-Tregs (Fr. III) were the highest producers of IL-17 among CD4$^+$ T cells. These results support recent findings in mice that FoxP3-RORγt double-positive CD4$^+$ T cells can convert into either Treg cells or Th17 cells (Yang et al., 2008a; Zhou et al., 2008). AHR was recently shown in mice to be critical for the differentiation of naive T cells to Th17 versus FoxP3$^+$ Treg cells (Quintana et al., 2008; Veldhoen et al., 2008). Our finding of upregulated AHR repressor in aTreg cells therefore suggests that differentiation of FoxP3$^-$CD4$^+$ T cells to aTreg cells might be regulated through the modulation of AHR activity by AHR repressor. Further study is required to determine how the expression amount of FoxP3 in each FoxP3$^+$ subpopulation contributes to the function of each subset (e.g., suppression and IL-17 production) through interaction with other molecules including RORC.

This study has revealed several key features of Treg cell-mediated suppression in vitro. First, challenging the commonly accepted notion that Treg cells are anergic in vitro, human Treg cells proliferate and die, although the degree of their proliferation is much lower than that of non-Treg cells when Treg cells and non-Treg cells are separately stimulated and compared. Further, the hypoproliferation observed with CD25^{hi}CD4$^+$ T cells can be attributed, in part, to the suppression of rTreg cell proliferation by aTreg cells and also to the death of the latter. These findings mean that thymidine uptake by whole cocultured cells in Treg cell assay may not be accurate to monitor responder cell proliferation in the presence of Treg cells. Second, CTLA-4 expression in aTreg cells, but not in rTreg cells, suggests that aTreg cells are the main effectors of suppression as shown by the fact that Treg cell-specific deficiency impairs Treg cell suppressive function in vivo and in vitro in mice (Wing et al., 2008). Further, FoxP3$^+$ Treg cells out-compete naive T cells in in vitro aggregation around dendritic cells and downregulate their expression of CD80 and CD86 in a CTLA-4-dependent fashion (Onishi et al., 2008). It is likely in humans that, upon activation, rTreg cells differentiate to aTreg cells and exert suppression in vitro through these mechanisms. As another possibility, rTreg and aTreg cells might use different suppressive mechanisms by secreting different immunosuppressive cytokines such as IL-10 and TGF-β (Ito et al., 2008). Our microarray analysis indeed indicates that aTreg cells are more active in IL-10 transcription but less active in TGF-β transcription than rTreg cells. Further study is required to determine whether Treg cells use multiple suppressive mechanisms depending on their differentiation status (Sakaguchi et al., 2008).

Finally, supporting physiological and clinical relevance of distinguishing subpopulations of FoxP3$^+$ T cells, rTreg and aTreg cells can be clearly identified with different proportions in cord blood of healthy newborns, PBL of aged individuals, and patients with SLE or sarcoidosis. In cord blood, we unexpectedly found a small but always detectable population of CD45RA^{lo}Ki-67$^+$FoxP3^{hi}CD4$^+$ T cells that corresponded to adult aTreg cells. This finding suggests that even in fetuses, natural rTreg cells are constantly activated by endogenous self antigens and exogenous antigens derived from maternal circulation. An opposite trend exists in aged donors, who had high proportions of aTreg cells and low but still detectable proportions of rTreg cells. Because of thymus involution observed in aged individuals, one can speculate that, like conventional naive CD4$^+$ T cells (Vrisekoop et al., 2008), rTreg cells can be generated in the periphery in aged individuals to compensate for decreased thymic production of Treg cells; alternatively, but not exclusively, aTreg cells may homeostatically expand to counterbalance the lack of rTreg cells in the periphery. Under pathological conditions, a high prevalence of aTreg cells and a decrease in the rTreg cell population in sarcoidosis suggests that rTreg cells may be swiftly converted into aTreg cells immediately after having emigrated from the thymus or having been peripherally generated. In contrast, in active SLE, the number of aTreg cells decreased while that of rTreg cells remained normal or increased, with a notable increase in FoxP3^{lo}CD4$^+$ non-Treg cells. This also confirms the FoxP3^{lo}CD45RA$^-$ memory/effector-like non-Treg cell subset as a discrete population among FoxP3$^+$ CD4$^+$ T cells. Further functional analysis is required to interpret these anomalies and variations in disease states (Taflin et al., 2009). Yet, analysis of Treg cell function by dissecting FoxP3$^+$ cells into three subpopulations is instrumental for understanding pathophysiology of immunological diseases.

In conclusion, we propose a definition of human FoxP3$^+$ Treg cell subsets based on in vitro and in vivo features of FoxP3-expressing CD4$^+$ T cells. Functional and numerical analysis of each subset will help to understand and control immune responses in normal and disease states.

EXPERIMENTAL PROCEDURES

Human Samples

Blood samples were obtained from young healthy adult volunteers (18–40 years old), from aged control donors (79–90 years old), and from active sarcoidosis or active SLE patients and cord blood samples from full-term neonates who had no hereditary disorders, hematologic abnormalities, or infectious complications. Aged donors had no acute or chronic inflammatory or infectious disease, ongoing thrombosis, or neoplasia. Diagnosis of active SLE and sarcoidosis were made according to previously described criteria (Miyara et al., 2005, 2006). All patients were newly diagnosed and not medicated with steroid or immunosuppressant. The study was done according to the Helsinki declaration with the approval from the human ethics committee of the Institute for Frontier Medical Sciences, Kyoto University and from Comité Consultatif de Protection des Personnes dans la Recherche Biomédicale of Pitié-Salpétrière Hospital, Paris. Human peripheral blood PBMC were prepared by Ficoll gradient centrifugation. Lymphocyte subpopulations was isolated by a MoFLo cell sorter (Dako) after positive magnetic cell separation of CD4$^+$ T cells by CD4$^+$ T cell MACS beads (Miltenyi Biotec). Purity of isolated cells was always >95% (Figure S1). Autologous CD14$^+$ and CD19$^+$ cells positively selected by mixed MACS and irradiated (50 Gy) were used as accessory cells.

Mice

NOG mice described previously (Hiramatsu et al., 2003) were injected intravenously with 3.5–5 × 10^7 human PBMCs. The mice were maintained in our animal facility and treated in accordance with the guidelines of Kyoto University.

Flow Cytometry

Freshly obtained or in vitro cultured lymphocytes and human lymphocytes isolated from NOG mouse spleens were stained with anti-hCD4 (-PerCP-Cy5.5 from BD biosciences or -APC from R&D Systems), anti-hCD25 (-PE or -PE-Cy5 from BD), anti-hCD45RO (-PE from Beckman Coulter and PE-Cy7 from